COLÁISTE NA TRÍONÓIDE, BAILE ÁTHA CLIATH
Ollscoil Átha Cliath
TRINITY COLLEGE DUBLIN
The University of Dublin

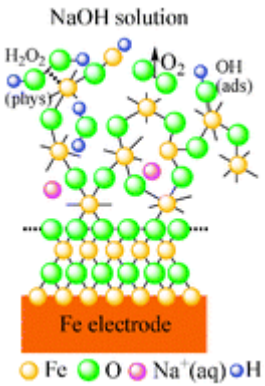

Lecture 4

Oxidative water splitting at metal oxide electrodes (SOWC's)

The Hydrogen Economy:
Hydrogen as an energy carrier.

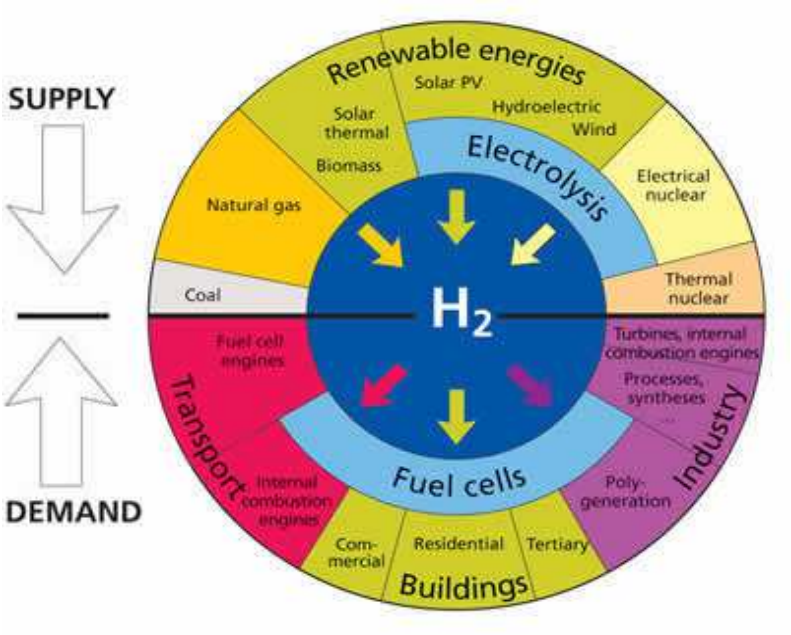

Electrical power sources are connected to two electrodes which are placed in water:

- Anode (oxidation OER):
  - $2\ H_2O(l) \rightarrow O_2(g) + 4\ H^+(aq) + 4e^-$
- Cathode (reduction HER):
  - $2\ H^+(aq) + 2e^- \rightarrow H_2(g)$

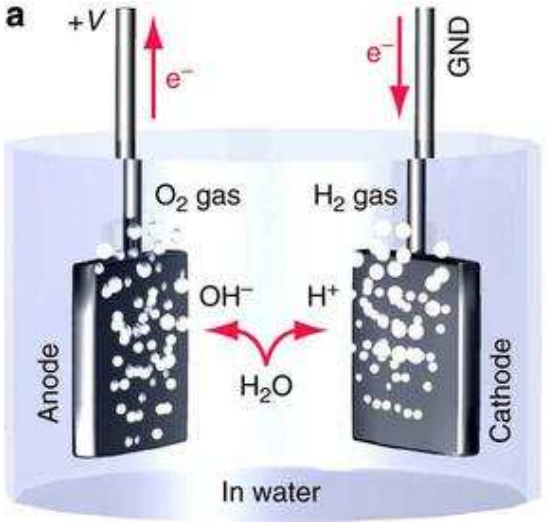

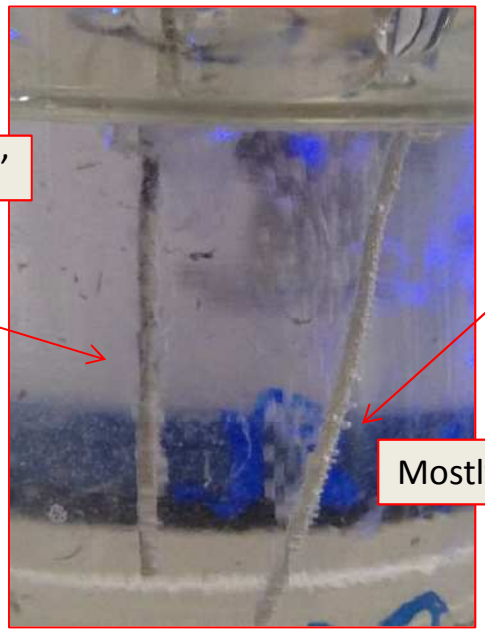

Cathodic Hydrogen Evolution Reaction (HER)

Acid: $2H_3O^+ + 2e^- \rightarrow H_2(g) + 2\ H_2O$
Base: $2H_2O + 2e^- \rightarrow H_2(g) + 2\ OH^-$

Simplest (therefore most studied) representative electro-catalytic reaction.
Multistep process involving adsorbed intermediates.

Volmer (V) : hydrogen adsorption or discharge step.

$H_3O^+ + M + e^- \rightarrow MH_{ads} + H_2O$

$H_2O + M + e^- \rightarrow MH_{ads} + OH^-$

Heyrovsky (H): Electrochemical Desorption step.

$MH_{ads} + H_3O^+ + e^- \rightarrow H_2(g) + M + H_2O$

$MH_{ads} + H_2O + e^- \rightarrow H_2(g) + M + OH^-$

Tafel (T) : Chemical Desorption step.

$MH_{ads} + MH_{ads} \rightarrow H_2(g) + 2M$

2 main mechanisms :

- **Volmer-Heyrovsky** (VH)
- **Volmer-Tafel** (VT).

Classical analysis assumes HER occurs on oxide free metal surface. However some metal oxide films are Stable under active HER conditions.

Anodic Oxygen Evolution Reaction (OER)

- Kinetically limiting step in water electrolysis cells and PEM fuel cell.
- Multistep multi-electron transfer reaction involving adsorbed intermediates.
- Overall reaction (alkaline medium)

$$O_2 + 2H_2O + 4e^- \leftrightarrows 4OH^-$$

E^0 = 0.303 V (vs. Hg/HgO)

- Krasil'shchikov (1963)

$$S + OH^- \leftrightarrows SOH_{ad} + e^-$$
$$SOH_{ad} + OH^- \leftrightarrows SO^-_{ad} + H_2O$$
$$SO^-_{ad} \leftrightarrows SO_{ad} + e^-$$
$$2SO_{ad} \rightarrow 2S + O_2$$

- Bockris Electrochemical Oxide (1956)

$$S + OH^- \leftrightarrows SOH_{ad} + e^-$$
$$SOH_{ad} + OH^- \leftrightarrows SO + H_2O + e^-$$
$$SO + SO \leftrightarrows 2S + O_2$$

- **Krasil'shchikov**/modification thereof, is pathway most often proposed for OER on metal / metal-oxide electrodes in alkaline solution.

- Depending on RDS can explain a variety of Tafel slopes.
- Modification permits concept of formation/decomposition of higher oxide – e.g. for Ni

$$OH^- \leftrightarrows OH_{ad} + e^-$$
$$OH_{ad} + OH^- \leftrightarrows O^-_{ad} + H_2O$$
$$2\ \beta\text{-}NiOOH + O^-_{ad} \leftrightarrows 2NiO_2 + H_2O + e^-$$
$$2NiO_2 + H_2O \leftrightarrows 2\ \beta\text{-}NiOOH + O_{ad}$$
$$O_{ad} + O_{ad} \rightarrow O_2$$

- OER at oxidized metal and metal oxide electrodes involves active participation of oxide.
- Acid/base behaviour of oxide important consideration .
- Concept of active surface or surfaquo groups important.

Anodic OER process is much more complex
And kinetically challenging than cathodic HER.
We focus attention on OER process at oxidized metal and metal electrodes.

Electrolytic generation of molecular di-oxygen

- Kinetically limiting step in water electrolysis cells and Electrowinning cell.
- Multistep multi-electron transfer reaction involving adsorbed intermediates.
- Need to understand details of Oxygen Evolution Reaction (OER) in order to optimize process at electrode surface
- Depending on RDS can explain a variety of Tafel slopes.
- Key mechanistic parameters are : **Tafel Slope** and **reaction order** wrt proton/hydroxide ion activity.
- OER at oxidized metal and metal oxide electrodes involves active participation of oxide.
- Acid/base behaviour of oxide important consideration .
- Concept of active surface or surfaquo groups important.

Anodic Oxygen Evolution Reaction (OER)

Table 2. Kinetic parameters derived for 5 most common OER mechanisms [169].

Rate-determining step		Langmuir				Temkin				
		$\frac{\partial E}{\partial \ln i}$		$\left[\frac{\partial \ln i}{\partial \ln C_{OH^-}}\right]_{E,\zeta}$[c]		$\frac{\partial E}{\partial \ln i}$				
	ν[b]	θ→0	θ→1	θ→0	θ→1	NA[d]	A[e]	NA[d]	A[e]	condition[f]
(I) Bockris's Oxide Path										
1. $M + OH^- \rightarrow MOH + e^-$	4	2RT/F		1						
2. $2MOH \rightarrow MO + M + H_2O$	2	RT/2F	∞	2	0	2RT/F		0.5		$r_{OH} \sim r_O$
						RT/F		1		$r_{OH} >> r_O$
3. $2MO \rightarrow 2M + O_2$	1	RT/4F	∞	4	0	RT/2F	RT/F	2	1	$K_2 \sim 1$
						RT/4F	RT/3F	2	1	$K_2 << 1$
(II) Bockris's Electrochemical Path										
1. $M + OH^- \rightarrow MOH + e^-$	2	2RT/F		1						
2. $MOH + OH^- \rightarrow MO + H_2O + e^-$	2	2RT/3F	2RT/F	2	1	2RT/F		1		$r_{OH} \sim r_O$
						RT/F		1.5		$r_{OH} >> r_O$
3. $2MO \rightarrow 2M + O_2$	1	RT/4F	∞	4	0	RT/2F	RT/F	2	1	$K_2 \sim 1$
						RT/4F	RT/3F	4	3	$K_2 << 1$
(III) Krasil'shchikov's Path										
1. $M + OH^- \rightarrow MOH + e^-$	2	2RT/F		1						
2. $MOH + OH^- \rightarrow MO^- + H_2O$	2	RT/F	∞	2	1	∞		1		$r_{OH} \sim r_{O^-}$
						2RT/F		1.5		$r_{OH} >> r_{O^-}$
3. $MO^- \rightarrow MO + e^-$	2	2RT/3F	2RT/F	2	0	2RT/F		0		$K_2 \sim 1$
						2RT/F		1		$K_2 << 1$
4. $2MO \rightarrow 2M + O_2$	1	RT/4F	∞	4	0	RT/2F	RT/F	2	1	$K_3 \sim 1$
						RT/4F	RT/3F	2	1	$K_3 << 1$
(IV) O'Grady's Path										
1. $M^z + OH^- \rightarrow M^zOH + e^-$	2	2RT/F		1						
2. $M^zOH \rightarrow M^{z+1}OH + e^-$	2	2RT/3F	2RT/F	1	0	2RT/F		0		$r_1 \sim r_2$[g]
						RT/F		0.5		$r_1 >> r_2$
3. $2M^{z+1}OH + 2OH^- \rightarrow M^z + H_2O + O_2$	1	RT/4F	∞	4	2	RT/2F	RT/F	4	3	$K_2 \sim 1$
						RT/4F	RT/3F	4	3	$K_2 << 1$
(V) Kobussen's Path										
1. $M + OH^- \rightarrow MOH + e^-$	1	2RT/F		1						
2. $MOH + OH^- \rightarrow MO + H_2O + e^-$	1	2RT/3F	2RT/3F	2	1	2RT/F		1		$r_{OH} \sim r_O$
						RT/F		1.5		$r_{OH} >> r_O$
3. $MO + OH^- \rightarrow MO_2H^-$	1	RT/2F	∞	3	1	∞		1		$K_2 \sim 1$
						RT/F		2		$K_2 << 1$
4. $MO_2H^- + OH^- \rightarrow MO_2^- + H_2O + e^-$	1	2RT/5F	2RT/F	4	1	2RT/F		1		$K_3 \sim 1$
						2RT/F		2		$K_3 << 1$
5. $MO_2^- \rightarrow M + O_2 + e^-$	1	2RT/7F	∞	4	0	RT/F	2RT/F	1	0.5	$K_4 \sim 1$
						RT/2F	2RT/3F	1	1.5	$K_4 << 1$

[a] Symmetry factors, i.e. β, γ, and δ, in all steps, were taken as ½. [b] Stoichiometric number. [c] ζ is the potential difference between the outer Helmholtz plane and the bulk of the solution. [d] Nonactivated desorption of O_2. [e] Activated desorption of O_2. [f] r is a coefficient determining the variation of heat of adsorption of a particular species with coverage. Unless stated, r values for each species were taken as equal. K_i is the equilibrium constant of the ith step. [g] r_1 and r_2 refer to r for M^zOH and r for $M^{z+1}OH$, respectively.

S. Rebouillat, M.E.G. Lyons, M.P. Brandon, R.L. Doyle, Int. J. Electrochem. Sci., 6 (2011) 5830-5917.

Rhodium redox chemistry: alkaline solution

Microdispersed hydrous oxide formed via potential cycling technique (similar to poly(aniline) deposition to form PME).

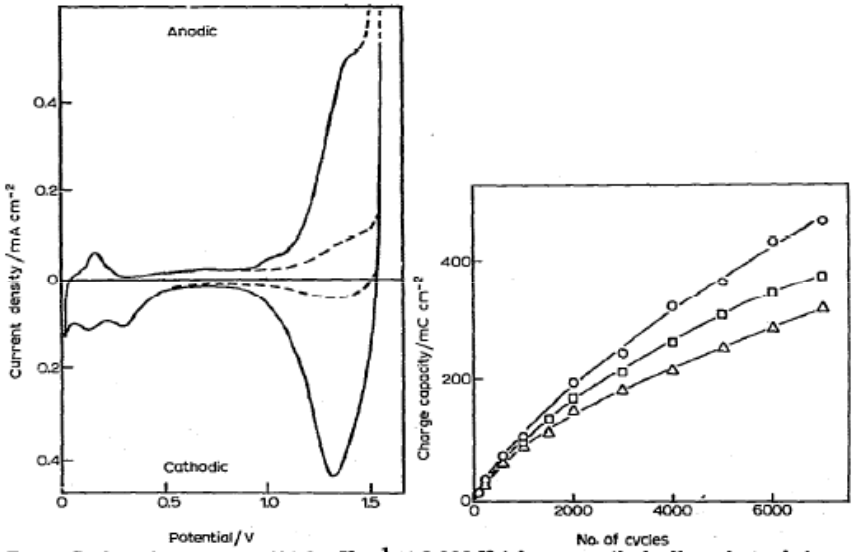

Fig. 1. Cyclic voltammogram (30.8 mV s^{-1} at 0.008 Hz) for a smooth rhodium electrode in 1.0 mol dm^{-3} NaOH at 25°C. The dashed line represents the behaviour of an unactivated electrode whereas the full line illustrates the charge enhancement produced on cycling the potential from 0.01 to 1.55 V for 40 s at 5 Hz.

Fig. 2. Increase in charge capacity associated with oxide formation at various temperatures as a function of the number of activating cycles. (○) 25°C; (□) 40°C; (△) 55°C. 1.0 mol dm^{-3} NaOH; activated at 5 Hz, 0.01 to 1.55 V.

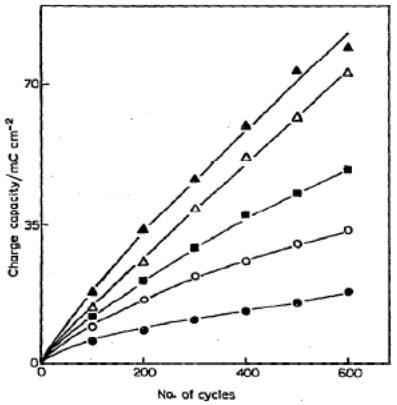

Fig. 7. Effect of sodium hydroxide concentration on the growth of charge capacity at a rhodium electrode in base. Concentration (mol dm^{-3}): (●) 0.1; (○) 0.25; (■) 0.5; (△) 1.0; (▲) 3.0. 5 Hz, 0.01 to 1.55 V, T = 25°C.

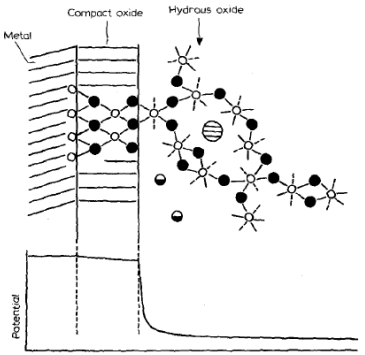

Fig. 1. Schematic representation of an in situ duplex oxide film formed on an iridium electrode under potential cycling conditions in acid. The suggested potential variation within the layers is outlined in the lower portion of this diagram. (○) iridium; (●) oxygen; (⊜) sulphate; (◒) hydrated proton.

L.D. Burke, E.J.M. O'Sullivan J. Electroanal. Chem., 93 (1978) 11.

L.D. Burke, E.J.M. O'Sullivan, J. Electroanal. Chem., 117(1981) 155.

Duplex layer model: oxide/solution interface.

OER at multicycled hydrous rhodium oxide modified electrodes.

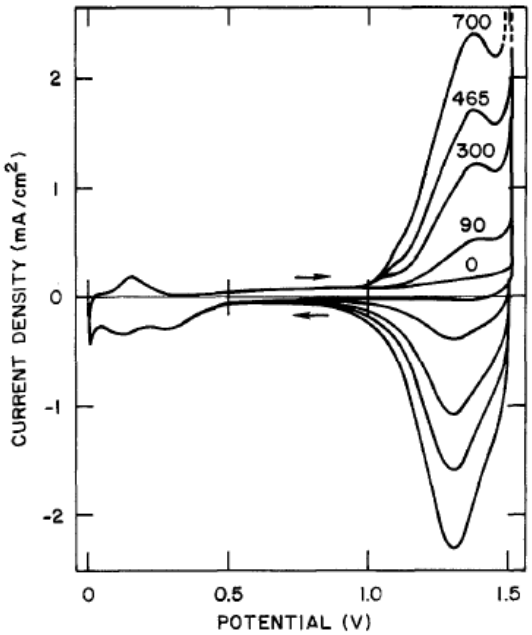

Fig. 1. Cyclic voltammograms (0.05 V s^{-1} sweep rate) for a rhodium electrode in 1.0 mol dm^{-3} NaOH after being subjected to various numbers of potential sweeps (0-1.50V, 0.15 V s^{-1}). Numbers refer to potential sweeps.

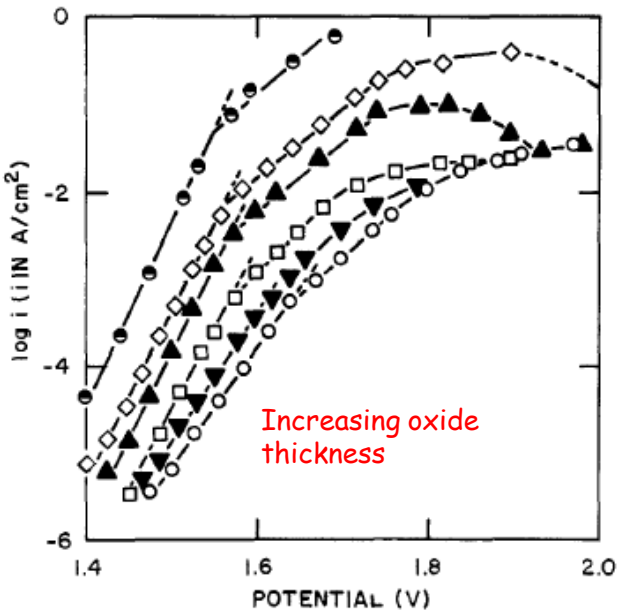

Fig. 2. Effect of thick oxide growth on the Tafel plots for oxygen evolution at Rh in 1.0 mol dm^{-3} NaOH at 25°C. Number of oxide growth cycles (0-1.55V, 3.0 V s^{-1}): (○) 0; (▼) 20; (□) 120; (▲) 600; (◇) 2100; (◓) 4500.

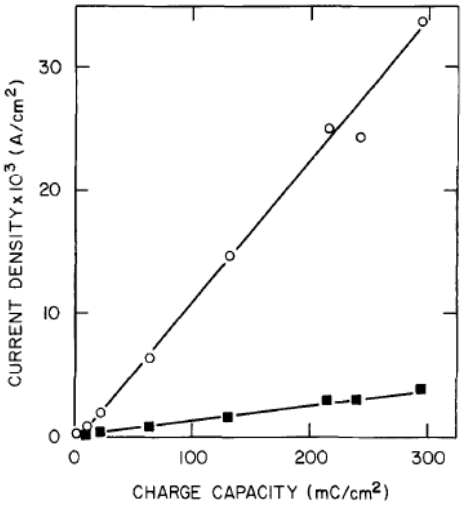

Fig. 4. Variation of oxygen evolution rate with increasing charge capacity of the cathodic peak at 1.35V for a Rh electrode in 1.0 mol dm^{-3} NaOH at 25°C: (■) 1.50V; (○) 1.55V.

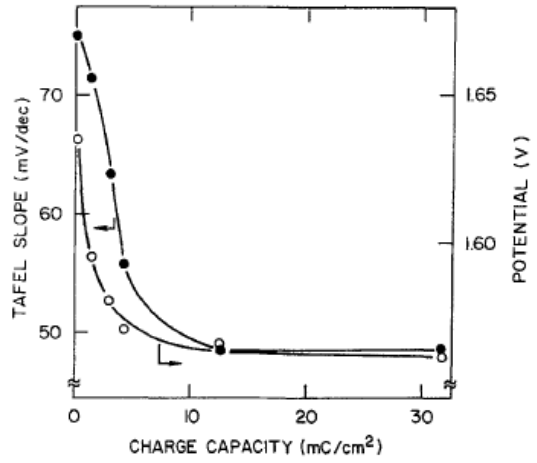

Fig. 3. Decrease in Tafel slope (●) and the potential (○) at which the changeover from the first to the second linear Tafel region (see Fig. 2) occurred with increasing charge capacity of the cathodic peak at ca. 1.35V in 1.0 mol dm^{-3} NaOH at 25°C.

OER activity & mechanism (shift in OER potential and decrease in Tafel slope) depends on charge capacity (thickness) of hydrous oxide layer.

O'Sullivan & Burke, J. Electrochem. Soc., 137 (1990) 466.

Anodic OER TEECE Group Activity

- Focus to date on kinetic and mechanistic studies on anodic OER for alkaline water electrolysis.
- Attention on oxidized transition metals, transition metal oxide coated electrodes (hydrous, electro-precipitated and thermally prepared).
- To date materials focus has been directed towards following systems:
  - Electrochemically prepared passive and hydrous Iron, Nickel, Cobalt oxy-hydroxide films.
  - Electrodeposited $Ni(OH)_2$ films on Au, GC and Pt support surfaces.
  - Thermally prepared single component oxides: NiO, RuO_2, IrO_2, Co_3O_4, MnO_2, on Ti and Ni support electrodes
  - Thermally prepared (from inorganic precursor salts annealed in air) mixed oxides: $Ru_xSn_{1-x}O_2$, $Ru_xIr_{1-x}O_2$, RuO_2/Co_3O_4 , $Ru_xTi_{1-x}O_2$, $Ir_xSn_{1-x}O_2$.
- Future attention on range of binary/ternary mixed DSA and nanostructured type metal oxides based on RuO_2 and IrO_2 incorporating cheap inactive metal oxides

- Electro-catalytic kinetics and mechanism with respect to anodic OER at Ni and Fe electrodes in aqueous base evaluated and quantified.
- Novel anodic water splitting OER mechanism proposed involving surf-aquo groups in hydrous oxide layer. OER onset potential depends on acid/base properties of hydrous oxide layer.
- Currently developing molecular scale model for detailed OER pathway in terms of interlinked surfaquo group model.
- Fe and Ni oxide materials are cheap and effective electrode materials for anodic water splitting.
- Next stage is to examine application of these oxide materials to Cathodic Oxygen Reduction Reaction (ORR) and hydrogen evolution reaction (HER). The latter topics are currently unexplored at hydrous oxide materials.
- Extending analysis to metal oxide films prepared via thermal decomposition of precursor & via sol/gel routes.

Pre-reduction at E = - 1.30V for t = 15 min, followed by 1 cycle between – 1.175
And 0.625 V in 1.0 M NaOH at 40 mV/s.

Oxidized metal electrode (not multicycled)

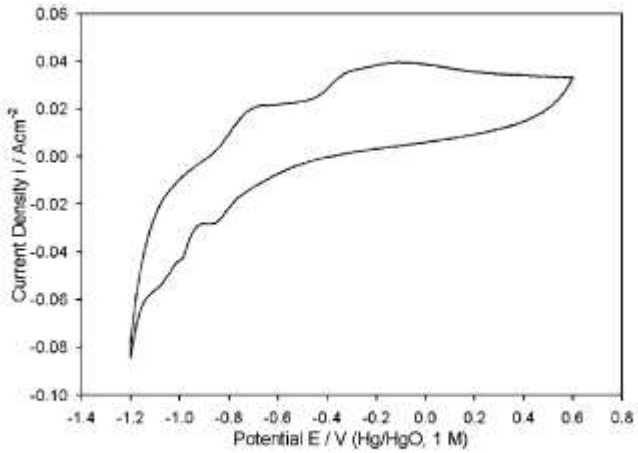

Fig. 12 Typical voltammetric profile for an aged iron electrode (see text for more details) recorded in 1.0 M NaOH at 40 mV s^{-1}.

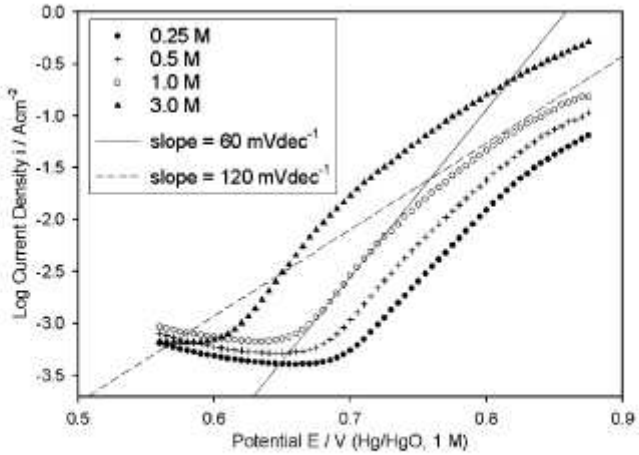

Fig. 13 *iR*-corrected steady state polarisation curves recorded in the direction of increasing potential for an aged iron electrode (as characterised voltammetrically in Fig. 12) in NaOH solutions of various concentration.

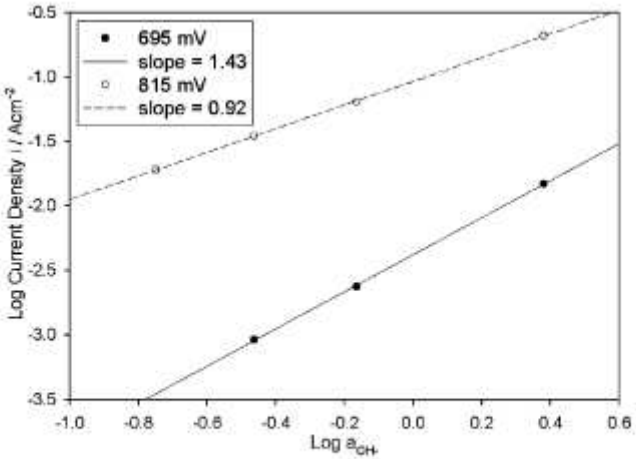

Fig. 14 Reaction order plots based upon the polarisation curves of Fig. 13, at the indicated potentials.

Aged electrode, severe cathodic pre-treatment: OER Kinetic parameters

Low overpotentials

b = 60 mV dec^{-1} = 2.303(RT/F)

m_{OH^-} = 3/2

High overpotentials

b = 120 mV dec^{-1} = 2.303(2RT/F)

m_{OH^-} = 1.0

Lyons & Brandon 2009

OER Kinetic Analysis: Model A Lyons 1984

$S + OH^- \rightarrow SOH + e^-$ (AI)
$SOH + OH^- \rightarrow SO^- + H_2O$ (AII)
$SO^- + OH^- \rightarrow SO_2H^- + e^-$ (AIII)
$SO_2H^- + OH^- \rightarrow S + H_2O + O_2 + 2e^-$ (AIV)

S = electrocatalytically active iron
surfaquo group = stabilized Fe(VI) moeity

QSSA, Langmuir Adsorption conditions:

$$i = \frac{4Fk_1^0 k_2 a_S a_{OH}^2 \exp[\beta F\eta/RT]}{k_{-1}^0 \exp[-(1-\beta)F\eta/RT] + k_2 a_{OH}}$$

Step (AI)
RDS
High overpotential

$$i \cong 4Fk_1^0 a_S a_{OH} \exp[\beta F\eta/RT]$$

Step (AII) RDS
Low overpotential

$$i \cong 4Fk_2 a_S a_{OH}^2 \{k_1^0/k_{-1}^0\} \exp[F\eta/RT]$$

Simple Kinetic analysis (Lyons 1984) predicts Correct Tafel slopes over entire η range, but predicts a reaction order m_{OH^-} of 2 at low η (instead of 3/2) and 1 at high η.

Dual Tafel Slope behaviour attributed to change in RDS as potential increases.

OER Kinetic Analysis: Model B Lyons & Brandon 2009

$S + OH^- \rightarrow S\text{-}OH + e^-$ (BI)

$S\text{-}OH + OH^- \rightarrow S\text{-}H_2O_2 + e^-$ (BII)

$S\text{-}H_2O_2 + OH^- \rightarrow S\text{-}OH_2^- + H_2O$ (BIII)

$S\text{-}H_2O_2 + S\text{-}HO_2^- \rightarrow O_2 + H_2O + OH^-$ (BIV)

$S\text{-}H_2O_2$ = physisorbed hydrogen peroxide

$0 < \theta_\Sigma < 0.8$

$0 < \gamma < 1 \quad \gamma = 1-\beta \quad \beta \cong 1/2$

Assume intermediate surface coverage of S-OH species. Pseudo –equilibrium condition & Temkin adsorption isotherm (interaction parameter g_j) assumed.

Assume at low η step (BII) is rate limiting.

$$f_\Sigma \cong k_2^0 a_{OH} \theta_{SOH} \exp\left[\frac{(1-\gamma) g_{SOH}\theta_\Sigma - \gamma g_{SH_2O_2}\theta_\Sigma}{RT}\right]\exp\left[\frac{\beta F\eta}{RT}\right]$$

$$f_\Sigma \cong k_2^0 a_{OH} \theta_{SOH} \exp\left[\frac{(1-\gamma) g_{SOH}\theta_\Sigma}{RT}\right]\exp\left[\frac{\beta F\eta}{RT}\right]$$

$g_{SOH} >> g_{SH_2O_2}$

$$f_\Sigma \cong f_2 = k_2^0 K^{1-\gamma} \theta_{SOH} a_{OH}^{2-\gamma} \exp\left[\frac{(1-\gamma+\beta)F\eta}{RT}\right]$$

$$b = \left(\frac{\partial \eta}{\partial \log f_\Sigma}\right)_{a_{OH}} = 2.303\left\{\frac{RT}{(1-\gamma+\beta)F}\right\} \xrightarrow{\gamma=\beta=1/2} \frac{2.303RT}{F}$$

$$m_{OH} = \left(\frac{\partial \ln f_\Sigma}{\partial \ln a_{OH}}\right)_\eta = 2-\gamma \xrightarrow{\gamma=1/2} 3/2$$

Assume step (BI) is in pseudo-equilibrium.

$$f_1 = f_{-1}$$

$$f_1 = k_1^0 a_{OH}(1-\theta_{SOH})\exp\left[-\frac{\gamma g_{SOH}\theta_\Sigma}{RT}\right]\exp\left[\frac{\beta F\eta}{RT}\right]$$

$$f_{-1} = k_{-1}^0 \theta_{SOH} \exp\left[\frac{(1-\gamma) g_{SOH}\theta_\Sigma}{RT}\right]\exp\left[-\frac{(1-\beta)F\eta}{RT}\right]$$

$$\left\{\frac{\theta_{SOH}}{1-\theta_{SOH}}\right\}\exp\left[\frac{g_{SOH}\theta_\Sigma}{RT}\right] \cong \exp\left[\frac{g_{SOH}\theta_\Sigma}{RT}\right] = \frac{k_1^0}{k_{-1}^0} a_{OH} \exp\left[\frac{F\eta}{RT}\right] = K a_{OH} \exp\left[\frac{F\eta}{RT}\right]$$

$$g_{SOH}\theta_\Sigma \cong RT \ln\{K a_{OH}\} + F\eta$$

At high η surface coverage conditions change to where $\theta_{SOH} = \theta_\Sigma \rightarrow 1$. Step (BII) still rate determining.
Langmuir adsorption pertains. Also $g_{SOH} \rightarrow 0$.

$$f_\Sigma \cong f_2 \cong k_2^0 a_{OH} \exp\left[\frac{\beta F\eta}{RT}\right]$$

$$b = 2.303\left\{\frac{2RT}{F}\right\}$$

$$m_{OH} = 1.0$$

OER Kinetics: Aged (EC polarization measurements) pre-reduced Fe electrodes (not multicycled).

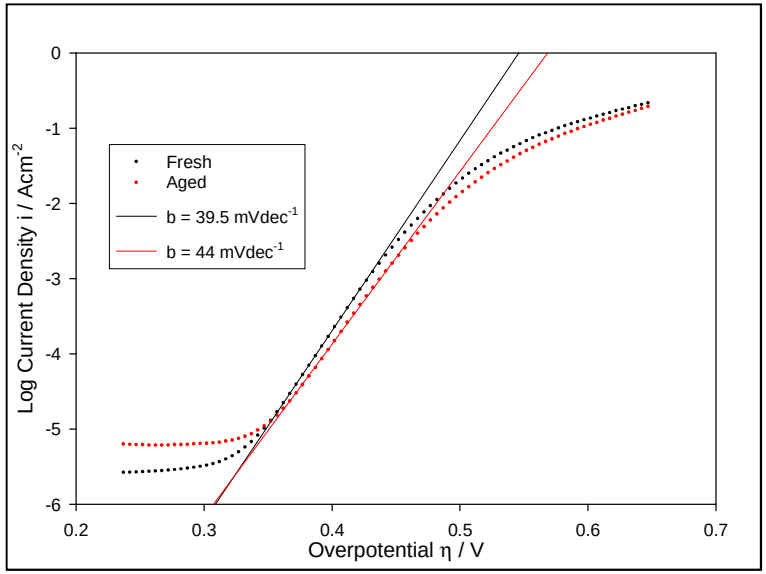

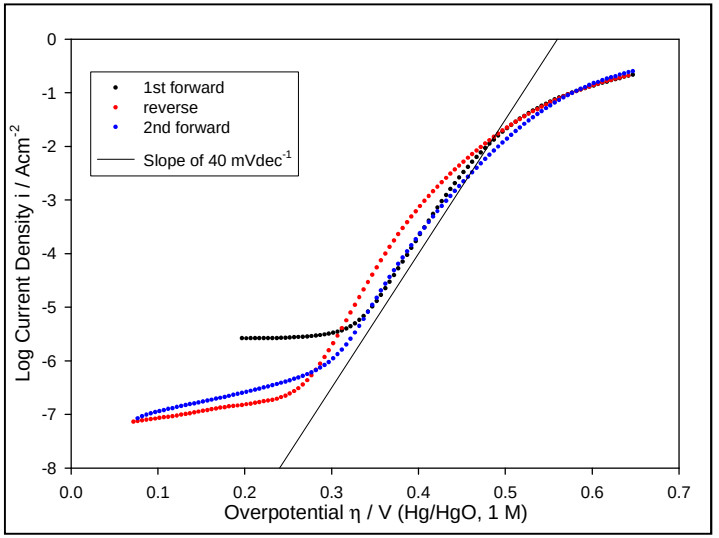

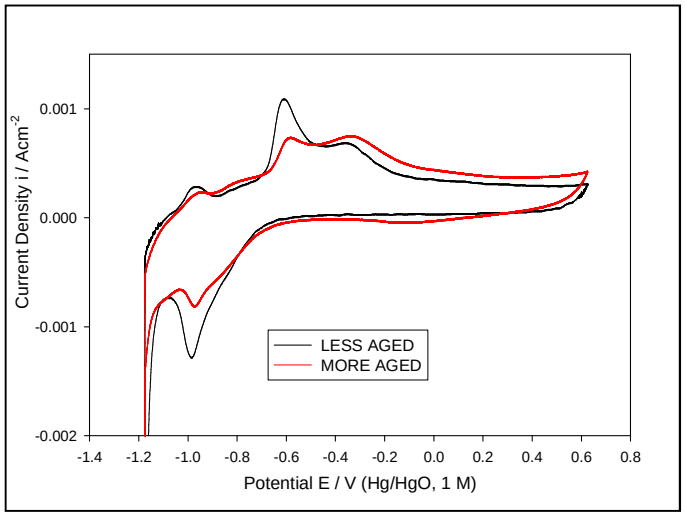

Peak A_4 becomes more enhanced on aging.
Compact anhydrous oxide chemistry
Dominates interfacial EC behaviour.
Is associated with increase in low overpotential
Tafel slope from ca. 40 mV to ca. 45-47 mV.

Pre-treatment: cathodic polarization at E = - 1.10V
In 1.0 M NaOH, t = 5 min, followed by single
Cycle at 40 mV/s between limits – 1.175 to 0.625 V.

OER Kinetics: Aged pre-reduced Fe electrodes (not multicycled).

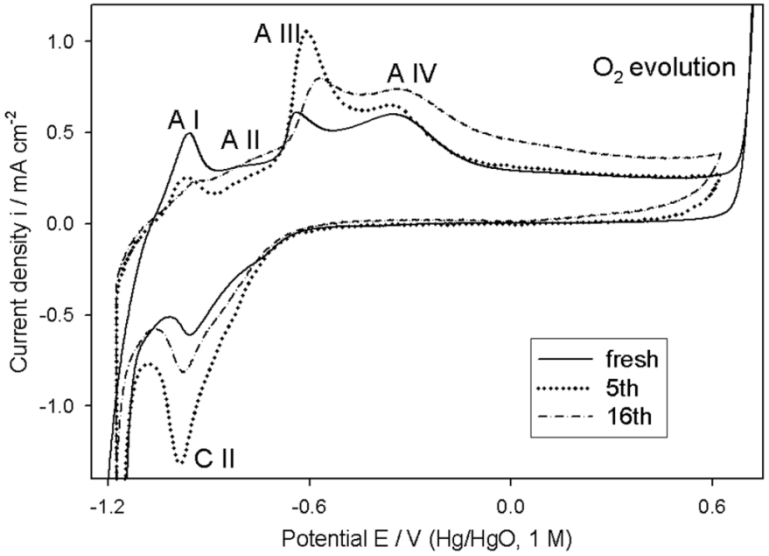

Cyclic voltammograms (1.0 M NaOH, scan rate = 40 mV s^{-1}) characterising an Fe electrode prior to its 1st, 5th and 16th utilisation in OER polarisation experiments.

Effect of oxide on OER Kinetics at oxidized aged Fe explained in terms of Conway-Meyer **dual barrier** model.

$$[Fe(VI)O_m(OH)_n]^{p-} + OH^- \rightarrow [Fe(VI)O_{m+1}(OH)_{n-1}]^{p-} + H_2O + e^-$$

$$[Fe(VI)O_{m+1}(OH)_{n-1}]^{p-} + OH^- \rightarrow [Fe(VI)O_m\underline{OOH}(OH)_{n-1}]^{p-} + e^- \text{ ...RDS}$$

$$[Fe(VI)O_m\underline{OOH}(OH)_{n-1}]^{p-} + OH^- \rightarrow [Fe(VI)O_m\underline{OO}(OH)_{n-1}]^{p-} + H_2O + e^-$$

$$[Fe(VI)O_m\underline{OO}(OH)_{n-1}]^{p-} + OH^- \rightarrow [Fe(VI)O_m(OH)_n]^{p-} + O_2 + e^-$$

$p = 2m+n-6$

$b \approx 2.303 \times 4RT/5F$
$m_{OH} \approx 1$

Low overpotential

Physisorbed peroxide intermediate model assumed.

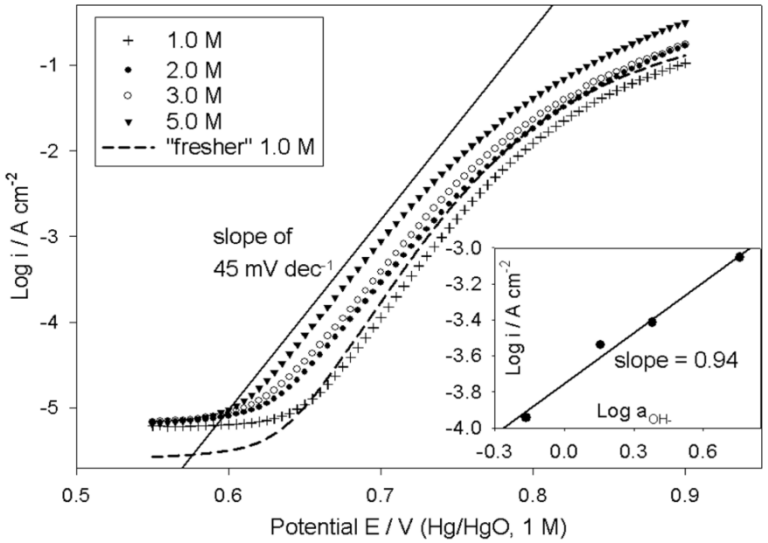

OER steady state polarisation curves for a pre-reduced Fe electrode in various NaOH solutions. The trace denoted as "fresher 1.0 M" was recorded for the same electrode in an earlier experiment, before satisfactory reproducibility with respect to Tafel slope had become established.
Inset – Reaction order plots constructed from the reproducible polarisation data at a potential of E = 0.7 V.

Conway-Meyer Dual Barrier Model

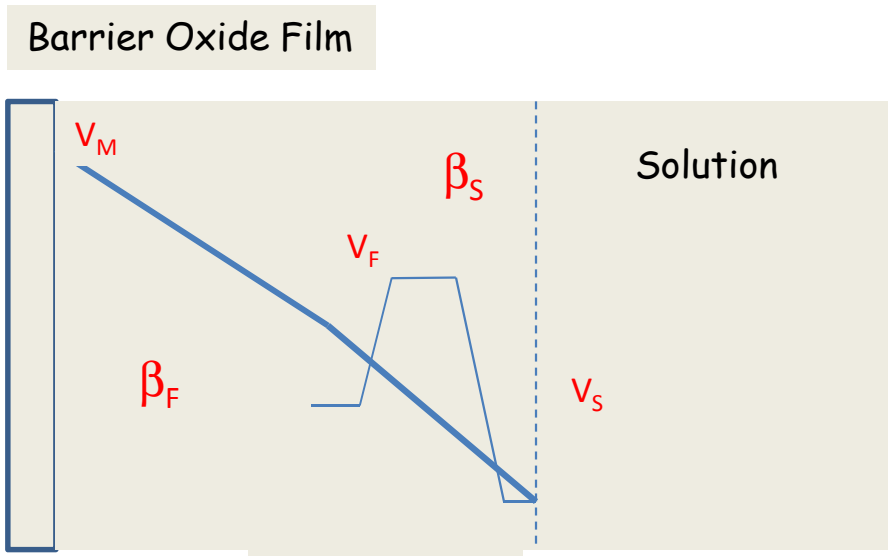

$$\beta_\Sigma \cong F(\beta)\beta_S = \left(\frac{\beta_F}{\beta_F + \beta_S}\right)\beta_S$$

$$b_{eff} \cong F(\beta)^{-1} b_S$$

$$m_{i,eff} \cong F(\beta) m_{i,S} = \left(\frac{\beta_F}{\beta_F + \beta_S}\right) m_{i,S}$$

Effective symmetry Factor $\beta_\Sigma = (\beta_F/(\beta_F+\beta_S))\beta_S$

Potential dependent field assisted charge Transfer across a barrier oxide film (process F) in series with interfacial charge transfer reaction (process S). Effective Symmetry factor (and hence Tafel slope) and reaction order is some fraction $F(\beta) = \beta_F/(\beta_F + \beta_S)$ of the true values.

$$f_\Sigma \cong k \prod_i (a_{is}^{m_{is}})^{\frac{\beta_F}{\beta_F+\beta_S}} \exp\left[\frac{\beta_\Sigma F \eta}{RT}\right]$$

$$b_{eff} = \left(\frac{\partial \eta}{\partial \log i}\right)_{a_S} = 2.303\left(\frac{RT}{\beta_\Sigma F}\right) = 2.303\frac{(\beta_F + \beta_S)}{\beta_F}\left(\frac{RT}{\beta_S F}\right)$$

$$m_{i,eff} = \frac{\beta_F}{\beta_S + \beta_F} m_{i,s}$$

Reaction order in absence of barrier

Effective reaction order

J.J. MacDonald, B.E. Conway, Proc. Roy. Soc., Ser.A, 269 (1962) 419-440.
R.E. Meyer, J. Electrochem. Soc., 107 (1960) 847-853.

Aged pre-reduced Fe electrodes
OER Kinetic analysis Incorporating DBM.

$S + OH^- \rightarrow S\text{-}OH + e^-$ (BI)
$S\text{-}OH + OH^- \rightarrow S\text{-}H_2O_2 + e^-$ (BII)
$S\text{-}H_2O_2 + OH^- \rightarrow S\text{-}OH_2^- + H_2O$ (BIII)
$S\text{-}H_2O_2 + S\text{-}HO_2^- \rightarrow O_2 + H_2O + OH^-$ (BIV)

Assume step (BII) is rate determining (low η values), and that dual barrier model pertains.
Analysis of barrier free situation suggests that b_S = 40 mV/dec (2.303(3RT/2F) and m_{OH} = 2.

$$f_\Sigma \cong Ka_{OH}^{\frac{2\beta_F}{\beta_F+\beta_S}} \exp\left[\frac{(1+\beta_\Sigma)F\eta}{RT}\right]$$

$$b_{eff} \cong \left(\frac{\partial\eta}{\partial \log i}\right)_{a_{OH}} = 2.303\left(\frac{RT}{(1+\beta_\Sigma)F}\right) = 2.303\left(\frac{RT}{\left(1+\frac{\beta_F\beta_S}{\beta_F+\beta_S}\right)F}\right) \xrightarrow{\beta_F\cong\beta_S=1/2} 2.303\left(\frac{4RT}{5F}\right) = 0.047\,V/dec$$

$$m_{OH,eff} \cong \left(\frac{\beta_F}{\beta_F+\beta_S}\right)m_{OH} = \frac{2\beta_F}{\beta_F+\beta_S} \xrightarrow{\beta_F\cong\beta_S=1/2} 1$$

Low overpotentials

Assume step (BI) is rate determining (high η values), and that dual barrier model pertains.
Analysis of barrier free situation suggests b_S = 0.120V /dec (2.303(2RT/F) and m_{OH} = 1.0.

$$f_\Sigma \cong Ka_{OH}^{\frac{\beta_F}{\beta_F+\beta_S}} \exp\left[\frac{\beta_\Sigma F\eta}{RT}\right]$$

High overpotentials

$$b_{eff} \cong 2.303\left(\frac{RT}{\beta_\Sigma F}\right) \cong 2.303\,\frac{(\beta_F+\beta_S)}{\beta_F}\left(\frac{RT}{\beta_S F}\right) = \frac{(\beta_F+\beta_S)}{\beta_F}b_S \xrightarrow{\beta_F\cong\beta_S=1/2} 2.303\left(\frac{4RT}{F}\right) \cong 0.235\,V/dec$$

$$m_{OH,eff} \cong \frac{\beta_F}{\beta_F+\beta_S}m_{OH} \xrightarrow{m_{OH}=1,\ \beta_F=\beta_S=1/2} 1/2$$

Not easy to check this prediction at high η.

OER Kinetics: Oxidized metal electrodes: Passive oxide films

M Brandon PhD Thesis 2008

Electrode	Experiment, b, m_{OH^-}	Dual barrier	b, m_{OH} for analysis	Isotherm L or T	Path-way
Ni no-pre-treat	2RT/3F – order not measurable	No	As listed left	L, $\theta \rightarrow 0$	C
Ni pre-reduced	2RT/3F, 1	No	As listed left	L, $\theta \rightarrow 0$	C
Ni pre-oxidised	2RT/3F, 1	No	As listed left	L, $\theta \rightarrow 0$	C
Co no-pre-treat	2RT/3F(5M)$\rightarrow$4RT/5F(1M)	low [OH^-]	-----	-----	-----
Co pre-reduced	4RT/5F, 1	Yes	2RT/3F, 2	L, $\theta \rightarrow 0$	E
Co aged low η	RT/F, 3/2	No	As listed left	T, $r_I >> r_{II}$	E
Co aged high η	2RT/F, 1	No	As listed left	L, $\theta \rightarrow 1$	E
Fe no-pre-treat	2RT/3F(1M)$\rightarrow$4RT/5F(5M)	high [OH^-]	-----	-----	-----
Fe pre-reduced (fresh)	2RT/3F – order not measurable	No	-----	-----	-----
Fe pre-reduced (aged)	4RT/5F, 1	Yes	2RT/3F, 2	L, $\theta \rightarrow 0$	E
Fe aged low η	RT/F, 3/2	No	As listed left	T, $r_I >> r_{II}$	E
Fe aged high η	2RT/F, 1	No	As listed left	L, $\theta \rightarrow 1$	E

Electrochemical Impedance Spectroscopy : Oxidized metal films anodic OER

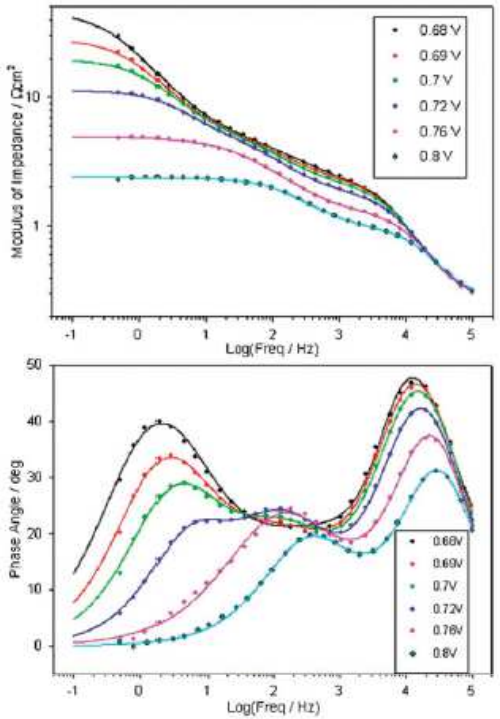

Fig. 15 Bode plots recorded at various potentials within the region of significant OER current density for an aged Fe electrode in 1.0 M NaOH solution. The raw data is represented by the circles, while the continuous lines plot the optimised transfer functions for the relevant equivalent circuit model (Fig. 17).

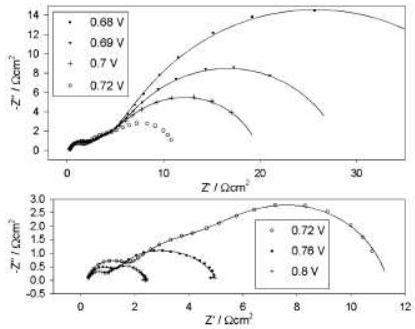

Fig. 16 Nyquist representations of the impedance data of Fig. 15. Again the continuous lines are generated by the results of the CNLS fitting process, while the discrete points represent the raw data.

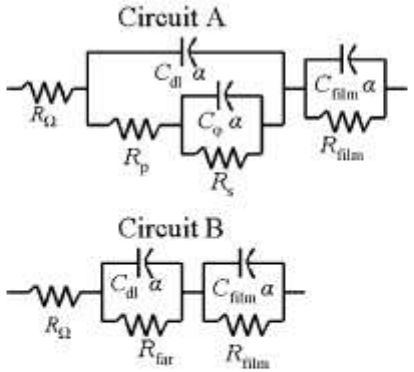

Fig. 17 Equivalent circuits used in the CNLS fitting of the impedance data of Fig. 15 and 16. Circuit A reduces to Circuit B at higher overpotentials and the latter is used for modelling the data recorded at 0.76 and 0.8 V. The meaning of R_{far} is discussed below (see eqn (9)).

Pseudo Tafel Plot from EIS Experiments

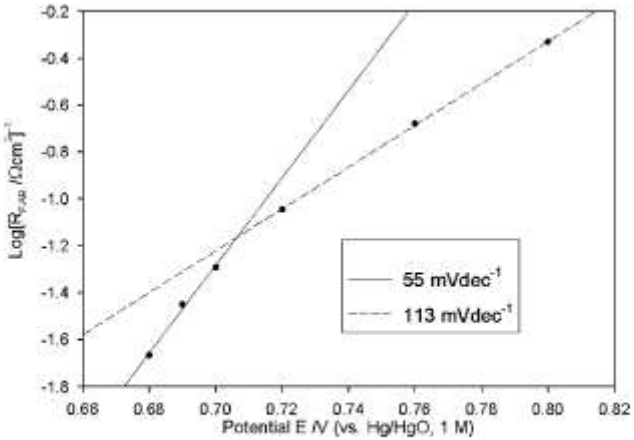

Fig. 18 Log $(R_{far})^{-1}$ *vs.* η plots constructed from the impedance data of Fig. 15.

Lyons Brandon
Physisorbed peroxide OER model incorporating Dual Barrier concept.

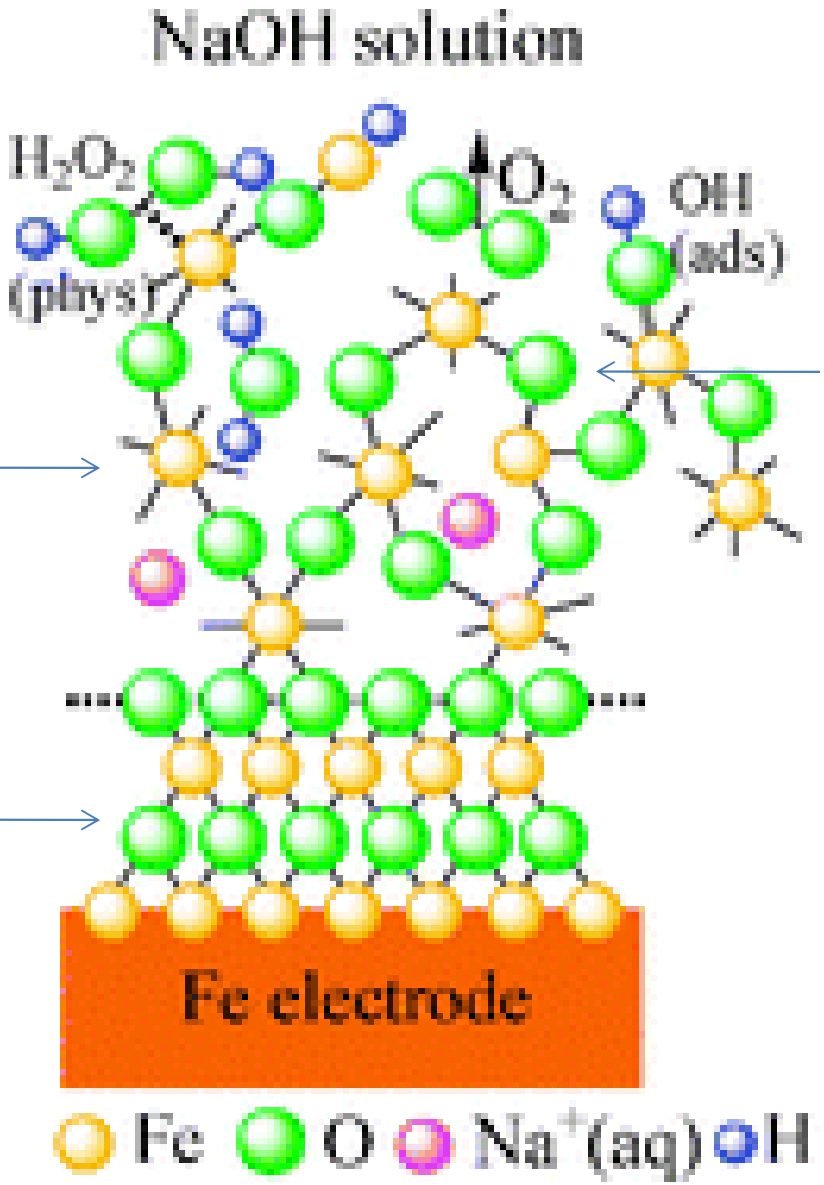

Interlinked surfaquo groups

Hydrous Oxide Layer

Compact Oxide Layer

Bockris, Otagawa, J. Phys. Chem.,87 (1983)2960
Bockris, Otagawa, J. Electrochem. Soc., 131 (1984) 290.

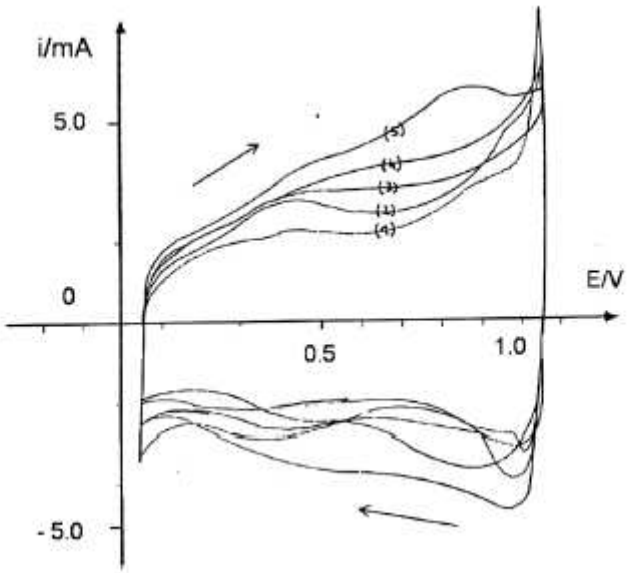

Fig. 1 Typical voltammetric profiles recorded in 1.0 mol dm^{-3} H_2SO_4 for a series of thermally prepared $Ir_xRu_{1-x}O_2$ coated Ti electrodes. Sweep rate: 20 mV s^{-1}. Mole fraction IrO_2: (1) 0, (2) 0.2; (3) 0.5; (4) 0.8; (5) 1.0. Potential range: 0.05 V to 1.05 V (*vs.* SCE). The inset directed arrows denote the direction of the forward and reverse potential sweeps.

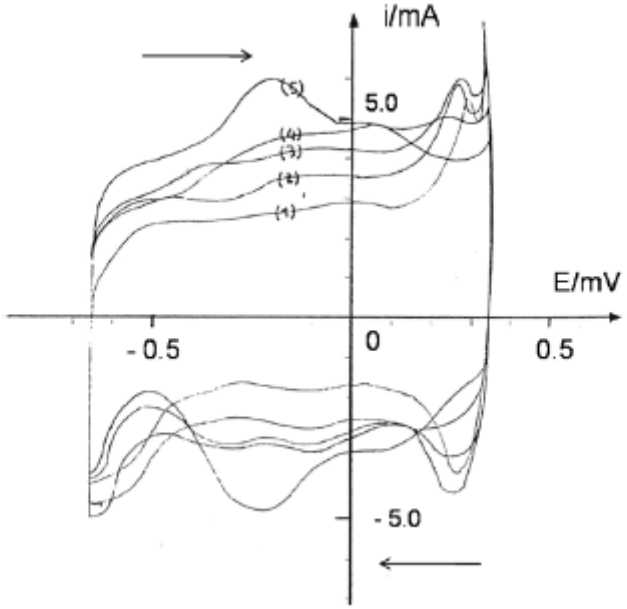

Fig. 2 Typical voltammetric profiles recorded in 1.0 mol dm^{-3} NaOH for a series of thermally prepared $Ir_xRu_{1-x}O_2$ coated Ti electrodes. Sweep rate: 20 mV s^{-1}. Mole fraction IrO_2: (1) 0, (2) 0.2; (3) 0.5; (4) 0.8; (5) 1.0. Potential range: –0.65 V to 0.35 V (*vs.* SCE). The inset directed arrows denote the direction of the forward and reverse potential sweeps.

It is well established that thermally prepared RuO_2 films exhibit three distinct redox processes involving $Ru^{III/IV}$, $Ru^{IV/VI}$ and $Ru^{VI/VII}$ surface redox transitions. The latter transformation which occurs at elevated anodic potentials prior to the onset of active oxygen gas evolution is most marked in base.

The chemistry of anhydrous iridium oxide involves a major charge storage $Ir^{III/IV}$ transition and an $Ir^{IV/VI}$ transition prior to the onset of active oxygen evolution.

We would therefore expect that the surface redox chemistry of a mixed oxide such as $Ir_xRu_{1-x}O_2$ in which both components are electroactive, would exhibit rather complex voltammetric behaviour.

Catalytic DSA MUDCRACK Morphology.

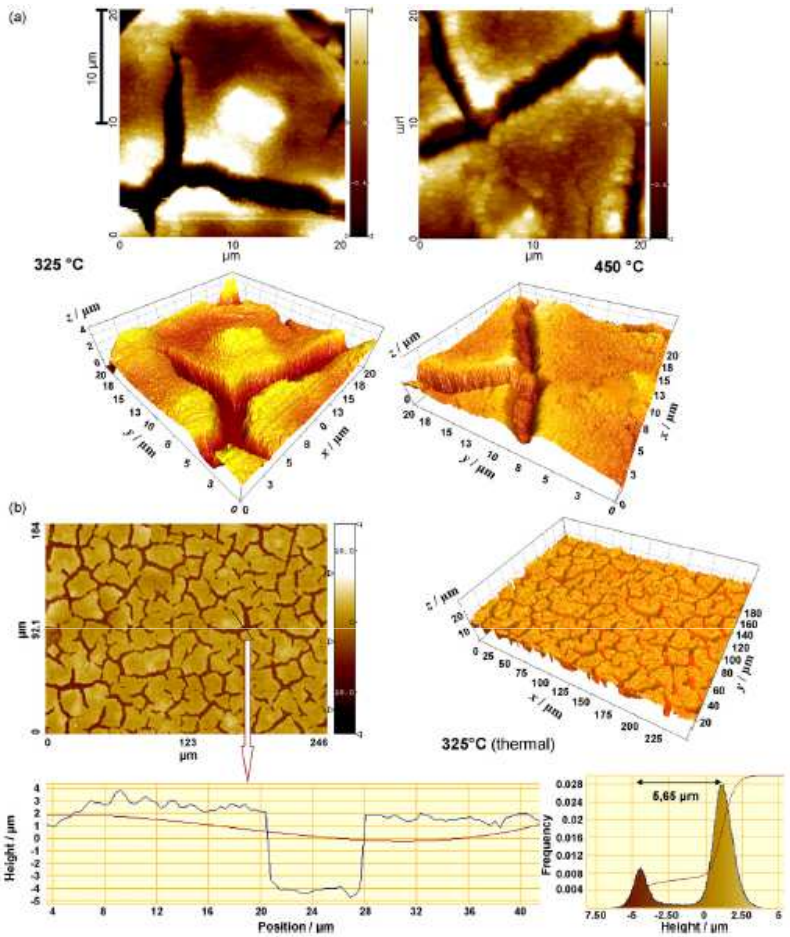

Fig. 2. (a) AFM-micrographs of RuO_2 electrodes prepared from $RuCl_3$ by thermal decomposition at 325 °C and 450 °C. Scan width 20 µm. (b) Visible light interferometry at the 325 °C RuO_2 electrode. Scan width 184 µm × 246 µm. Average layer thickness: 5.65 µm.

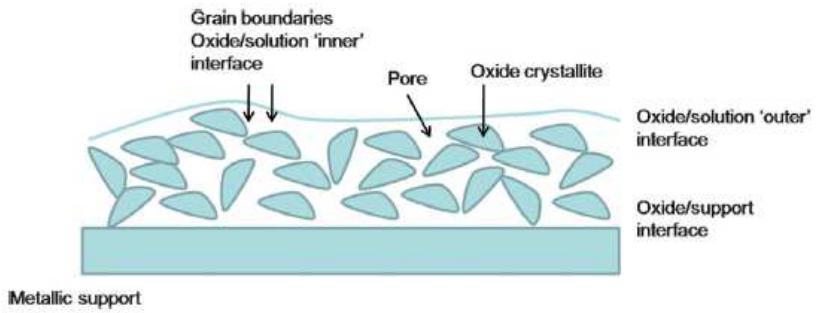

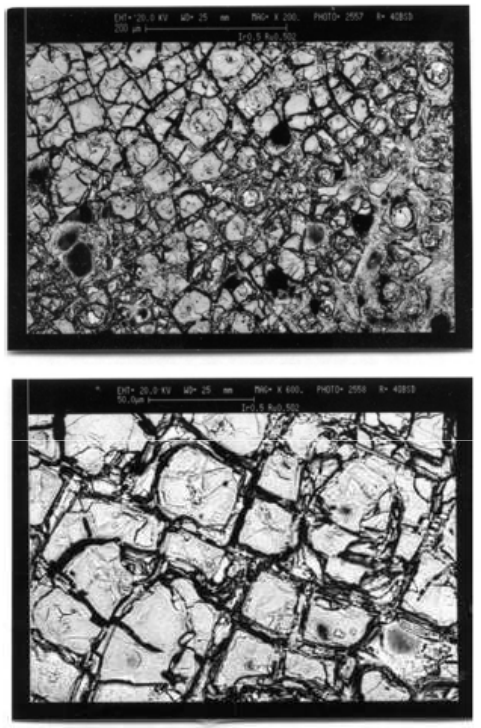

Fig. 5 SEM micrographs of an $Ru_{0.5}Ir_{0.5}O_2$ coated Ti electrode. (a) ×200, (b) ×600. The characteristic 'cracked' morphology is evident.

Surfaquo group concept

- Metal oxide surfaces in contact with aqueous solutions have a significant hydrophilic character. As an oxide interacts with water solvent molecules become bonded to the metal cations which exhibit Lewis acidity resulting in the transfer of a proton to a neighbouring oxygen site.
- Un-dissociated water molecules may also be present. Hence the oxide surface is extensively hydroxylated. It has been determined that only oxycations at certain sites (presumably sites of low coordination such as kink or ledge sites) are capable of participating in the redox reactions giving rise to the peaks observed in the recorded voltammetric response.
- The important factor seems to be the ability of the latter type of cations to extensively coordinate water molecules. Inactive ruthenium or iridium species would exhibit a higher degree of oxygen bridging type coordination and would presumably exist along terrace sites.

- These ideas emphazing the important role of hydration in determining the difference between active and inactive surface bonded groups led to the designation of the former as ***surfaquo groups***.
- Although the structure of such active surfaquo Groups is unknown it is very likely that the linkage to the surface involves one or more oxygen bridges to generate the following type of hydrous species (the bridging oxygen species being represented here by –O-):

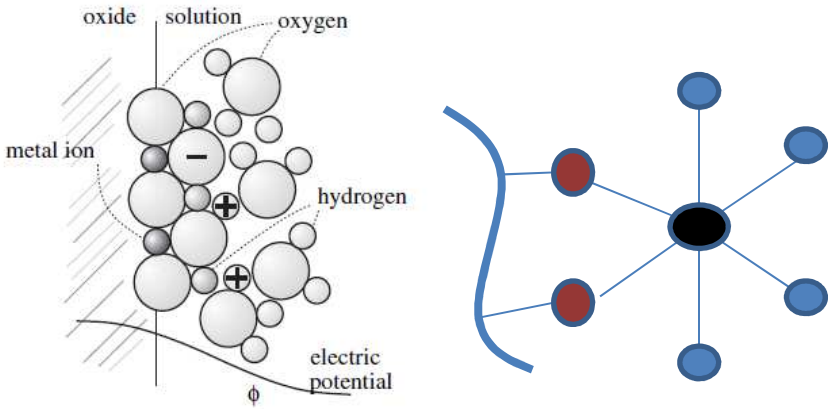

Fig. 9. Sketch of an oxide/aqueous solution interface.

Ru(VI) surfaquo groups

$(\text{-O-})_2\text{RuO}_2(\text{OH}_2)_2 \leftrightarrow (\text{-O-})_2\text{RuO(OH)}_2(\text{OH}_2) \leftrightarrow (\text{-O-})_2\text{Ru(OH)}_4$

Surfaquo group redox Chemistry:
RuO_2 surface.

$$(-O-)_2RuO_2(OH_2)_2 \leftrightarrow (-O-)_2RuO(OH)_2(OH_2) \leftrightarrow (-O-)_2Ru(OH)_4$$

$$Ru^{III/IV}: (-O-)_2RuOH(OH_2)_3 \rightarrow (-O-)_2Ru(OH)_2(OH_2)_2 + H^+ + e^-$$

$$Ru^{IV/VI}: (-O-)_2Ru(OH)_2(OH_2)_2 \rightarrow (-O-)_2Ru(OH)_4 + 2H^+ + 2e^-$$

$$Ru^{VI/VII}: (-O-)_2Ru(OH)_4 \rightarrow (-O-)_2RuO(OH)_3 + H^+ + e^-$$

$$(-O-)_2Ru(OH)_4 \leftrightarrow (-O-)_2RuO(OH)_3 + H^+ + e^- \text{ fast}$$

$$(-O-)_2RuO(OH)_3 \rightarrow (-O-)_2Ru^+O(OH)_3 + e^- \text{ slow rds}$$

$$(-O-)_2Ru^+O(OH)_3 \leftrightarrow (-O-)_2RuO(OH)_2 + O_2 + 2H^+ + 2e^- \text{ fast}$$

$$(-O-)_2RuO(OH)_2 + H_2O \leftrightarrow (-O-)_2Ru(OH)_4 \text{ fast}$$

OER Mechanism acid medium
1 M H_2SO_4

OER Mechanism basic medium
1M NaOH

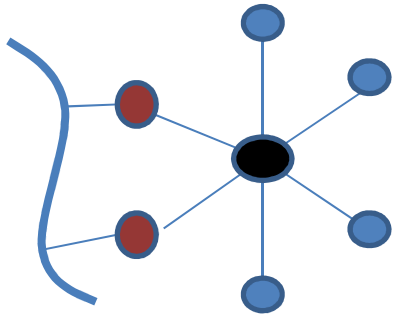

The chemistry of the OER is the chemistry of the surfaquo group.

$$(-O-)_2RuO^-(OH)_3 + OH^- \leftrightarrow (-O-)_2RuO{\cdot}O^-(OH)_2 + H_2O + e^- \text{ fast}$$

$$(-O-)_2RuO{\cdot}O^-(OH)_2 \rightarrow (-O-)_2RuO_2(OH)_2 + e^- \text{ slow rds}$$

$$(-O-)_2RuO_2(OH)_2 + 2OH^- \leftrightarrow (-O-)_2RuO_2(OH)_2 + O_2 + 2H^+ + 2e^- \text{ fast}$$

$$(-O-)_2RuO_2(OH)_2 + OH^- + H_2O \leftrightarrow (-O-)_2Ru(OH)_4 \text{ fast}$$

Anodic OER, Multicycled Fe aqueous alkaline solution.

$$E = a + b \log i$$

$$\frac{dE}{di} = \frac{b}{2.303}\frac{1}{i} + R_U A$$

Linear Plot : ΔE/Δi vs 1/i

60 mVdec^{-1} /40 mVdec^{-1} Tafel slope depends on base concentration/potential limits at which oxide layer is formed via RPM.

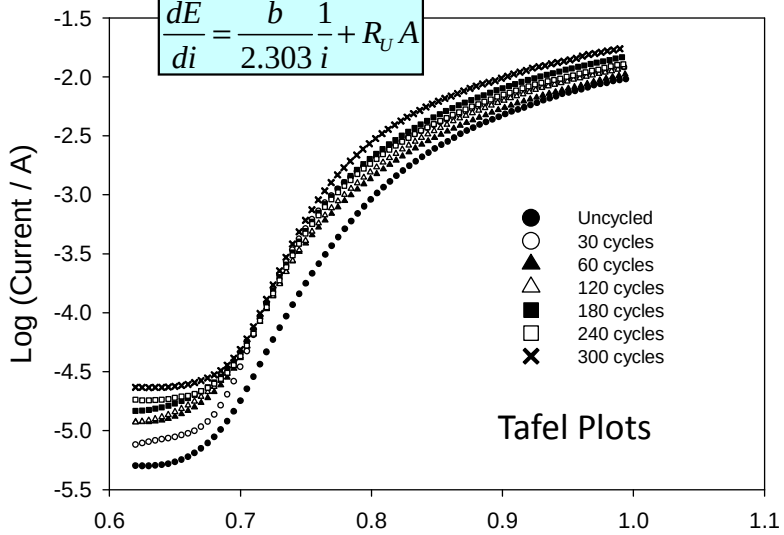

b = Tafel Slope
i = current density

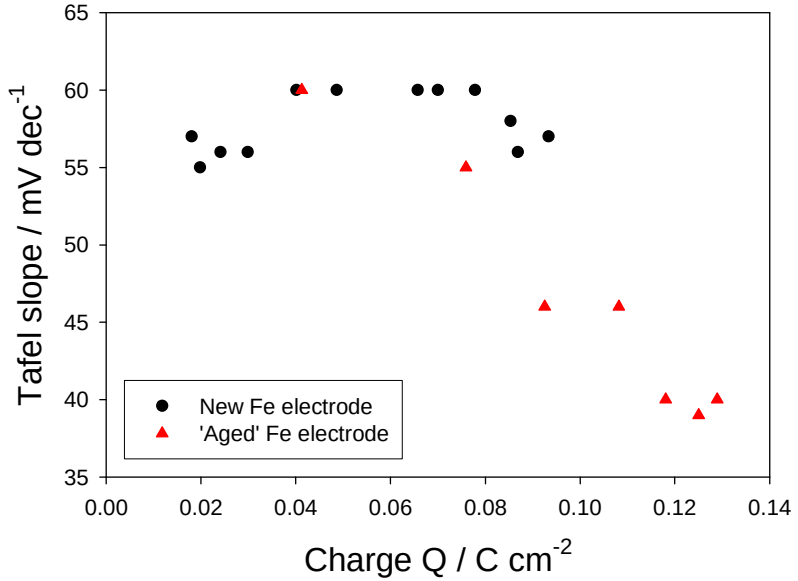

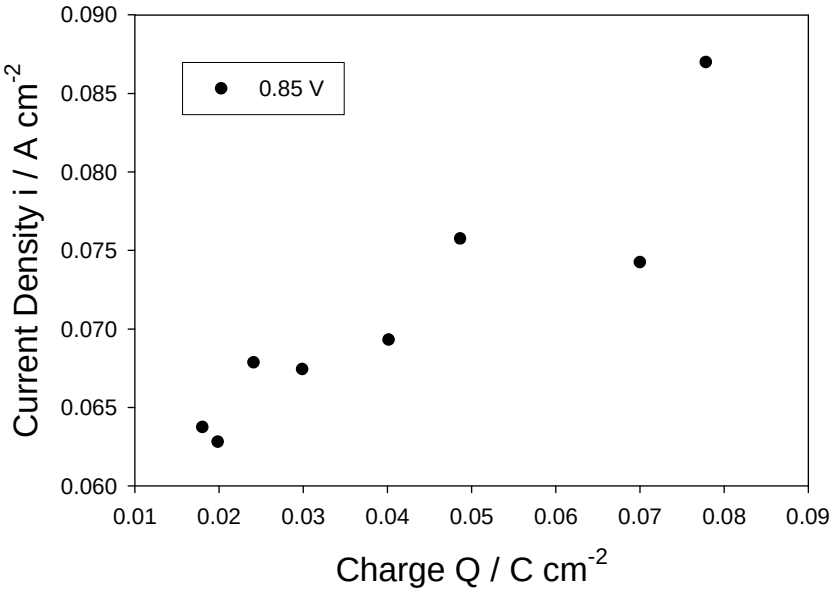

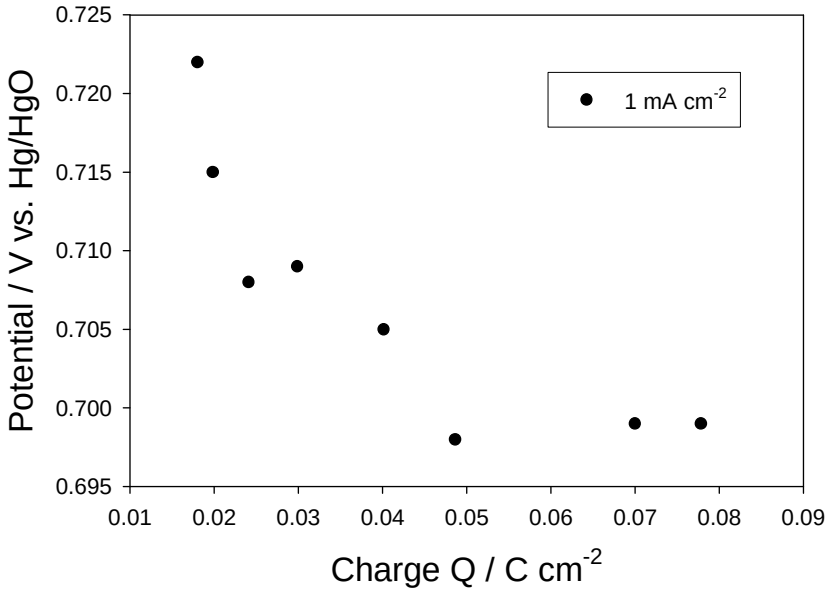

Hydrous Iron Oxide Electrodes.
OER Reaction Order Studies

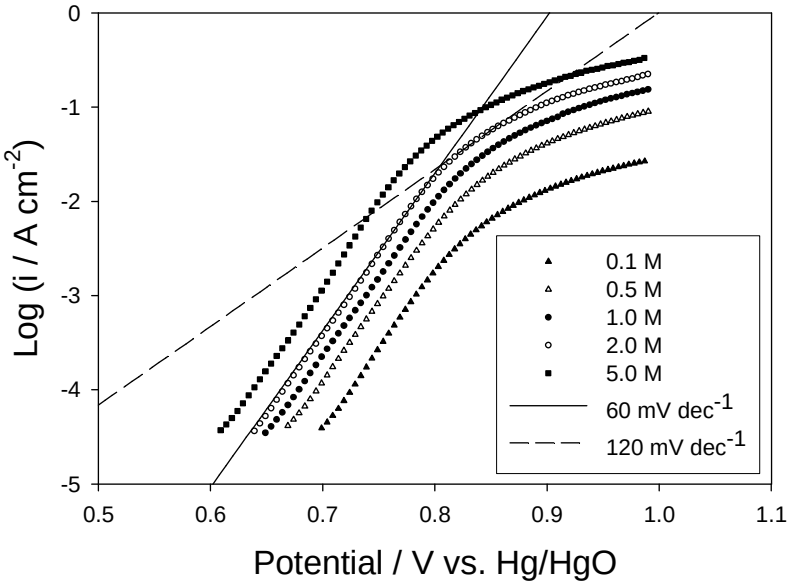

N = 120 cycles
Reaction order wrt OH^- activity ca. 0.9 (low TS region) and ca. 0.8 (high TS region).

Measure OER current density at fixed overpotential from analysis of Tafel Plots as function of OH^- ion activity.

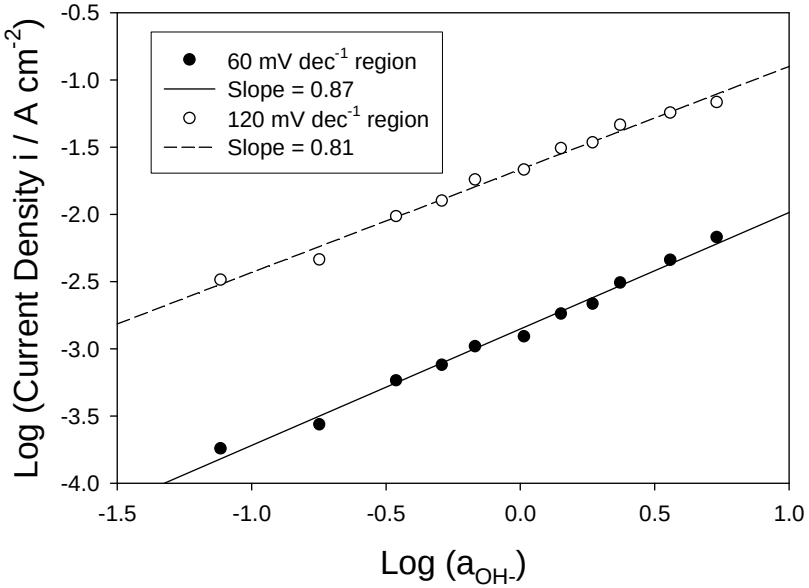

Ni in aqueous base: redox activity and OER behaviour.

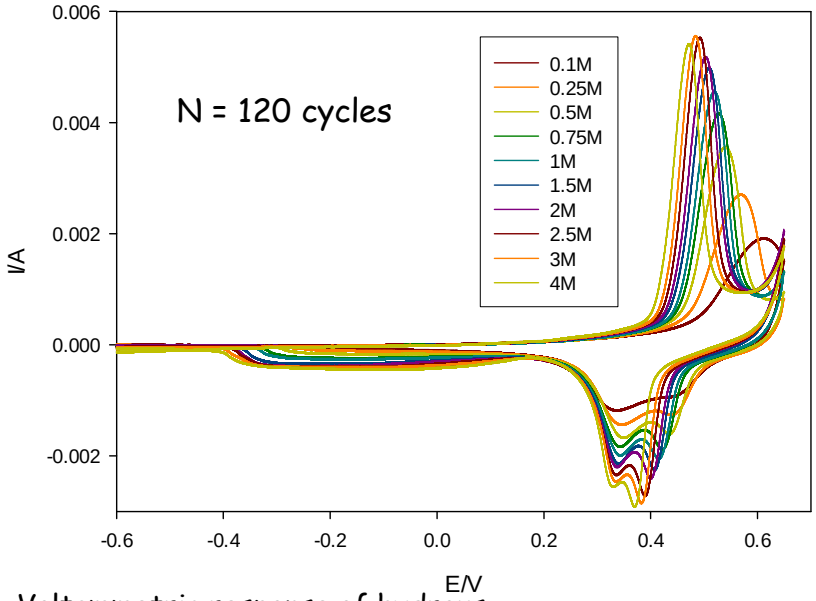

Voltammetric response of hydrous Ni oxide film as function of base Concentration.

Low potential : TS = 60 mV/dec.
High potential : TS = 120 mV/dec

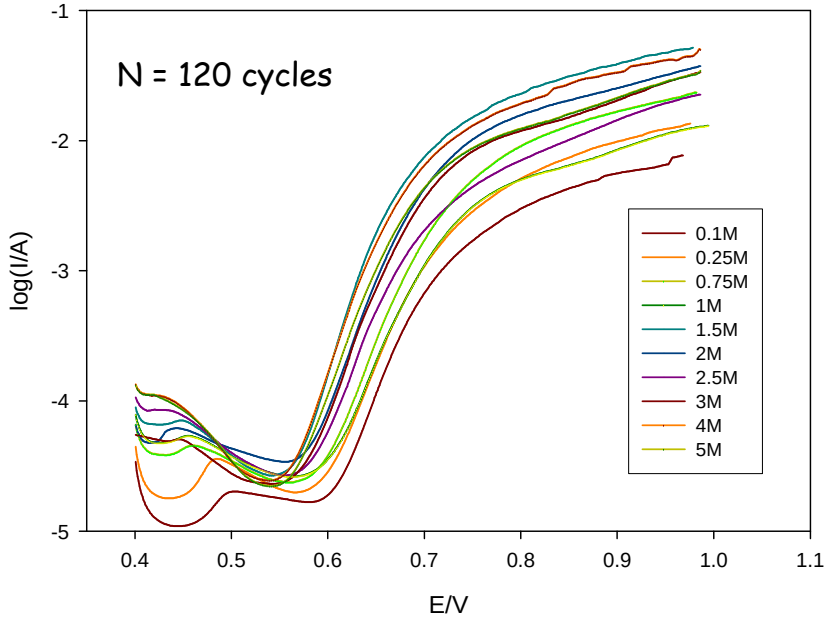

Tafel Plots for OER at Ni oxide layers grown via potential cycling (N = 120 cycles) in 1.0 M NaOH recorded as function of base concentration.

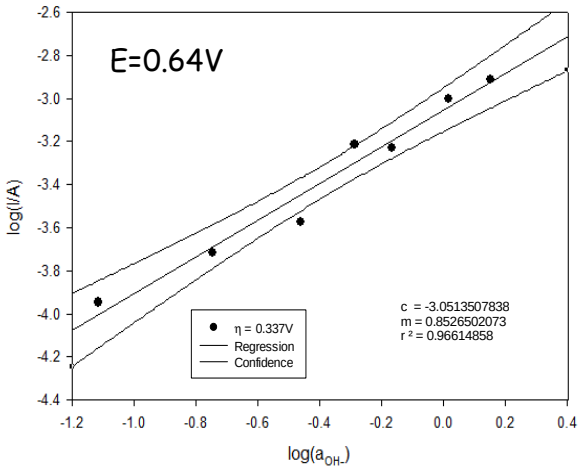

Ni oxide layer grown in 1.0 M NaOH. N = 120 cycles. Reaction order plot, low Tafel Slope Region.
m_{OH^-} = 0.85.

Ni oxide layer grown in 1.0 M NaOH. N = 120 cycles. Reaction order plot, high Tafel Slope Region.
m_{OH^-} = 0.82.

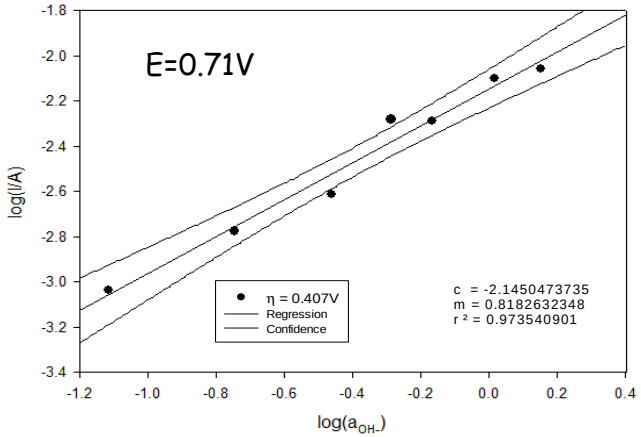

Effect of oxide charge capacity Q on OER catalytic efficiency: Ni in aqueous base.

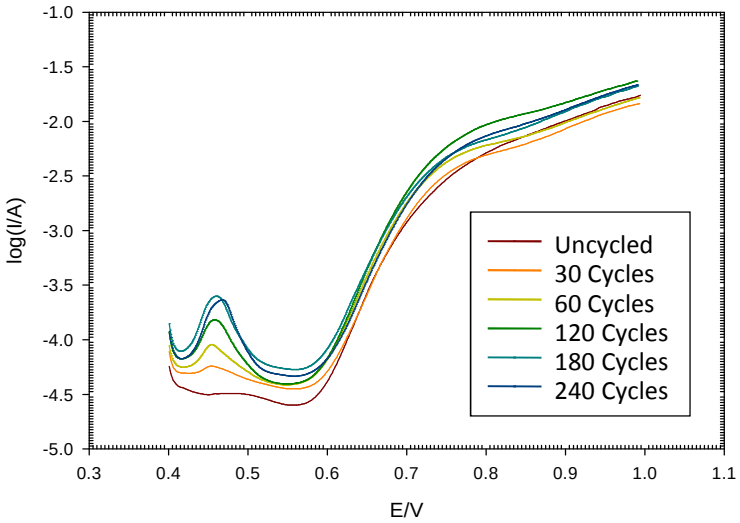

Tafel Plot OER as function of hydrous layer thickness (# cycles).

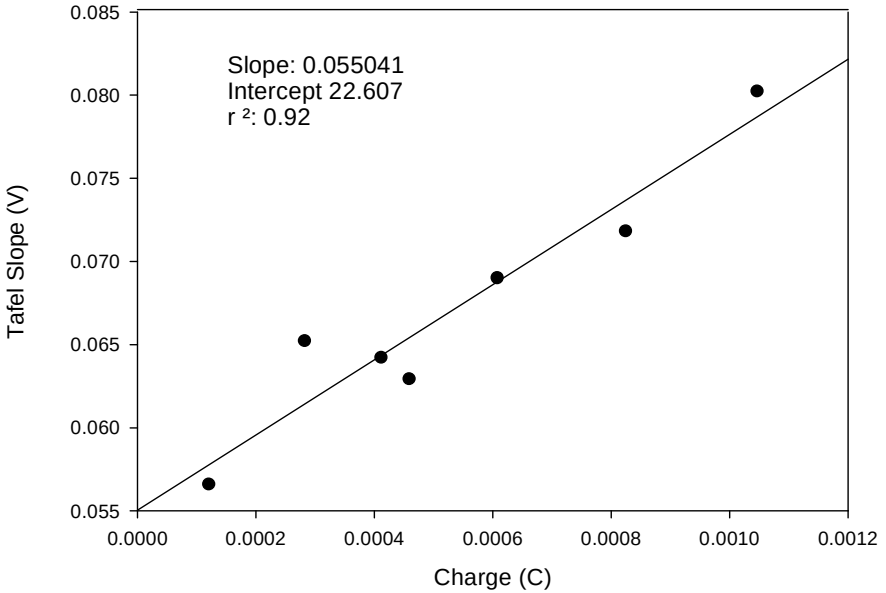

Variation of low overpotential Tafel Slope for OER at multicycled Ni oxide Electrode in 1.0 M NaOH as a function of oxide charge capacity Q (thickness).

Low overpotential Tafel Slope increases in a linear manner with increasing hydrous oxide charge capacity.

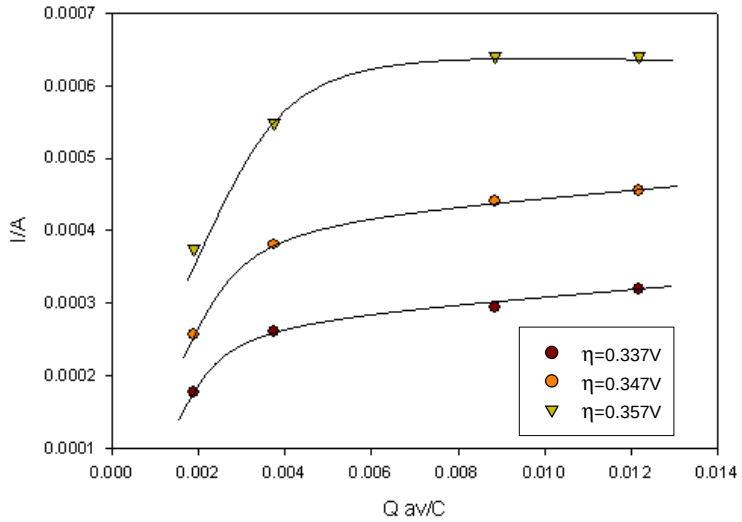

Oxygen evolution rate at fixed potential at oxide coated Ni in 1.0 M NaOH as function of redox charge storage capacity of hydrous layer.

(a) M.O'Brien, L. Russell, I. Godwin, R.L. Doyle, and M.E.G. Lyons, Redox switching and oxygen evolution at hydrous nickel oxide in aqueous alkaline solution, Electrochemical Society Transactions, Spring Meeting Seattle , USA, 2012, In press.

(b) M.E.G. Lyons, L. Russell, M. O'Brien, R.L. Doyle, I. Godwin, M.P. Brandon, Redox switching and oxygen evolution at hydrous oxyhydroxide modified nickel electrodes in aqueous alkaline solution: Effect of hydrous oxide thickness and base concentration. Int. J. Electrochem. Sci., 7 (2012) 2710-2763.

EIS Measurements : Hydrous iron oxide film

R.L. Doyle 2012, sub

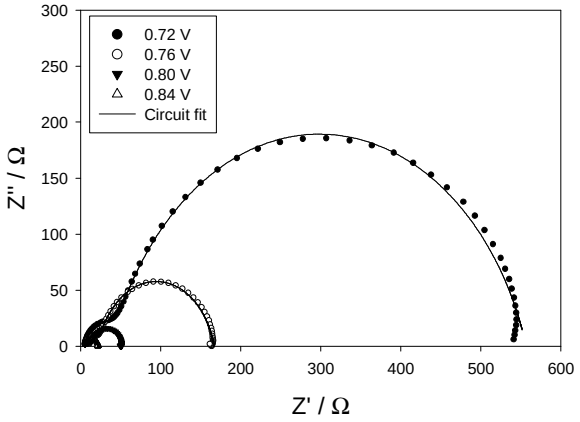

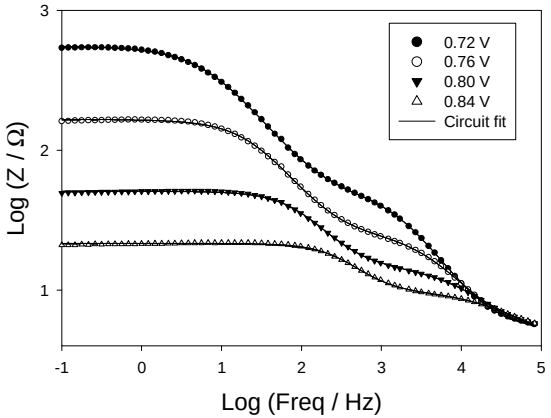

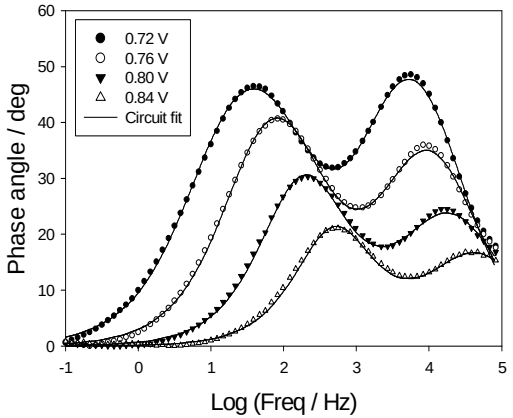

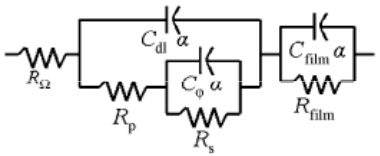

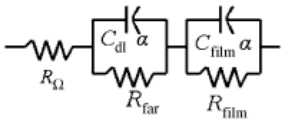

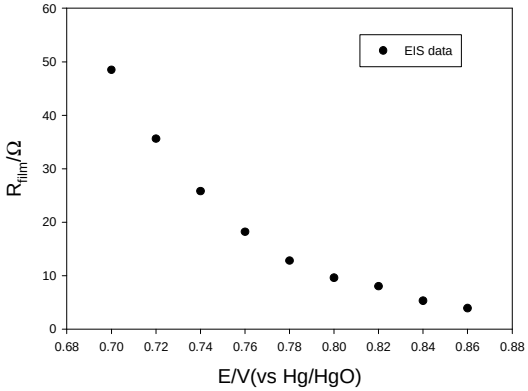

E / V	R_{Ω} / Ω	C_{dl} / µF cm^{-2} (α)	R_{far} / Ω	C_{film} / µF cm^{-2} (α)	R_{film} / Ω
0.70	5.1500	551 (0.78)	858.5	42.7 (0.90)	48.5
0.72	5.1340	560 (0.80)	516.1	45.4 (0.89)	35.6
0.74	5.0510	554 (0.83)	281.0	54.6 (0.86)	25.8
0.76	4.9600	567 (0.86)	143.4	66.8 (0.84)	18.2
0.78	4.8750	576 (0.87)	71.9	77.0 (0.82)	12.8
0.80	4.6430	536 (0.90)	36.8	112.0 (0.78)	9.6
0.82	4.1190	464 (0.93)	19.5	258.0 (0.69)	8.0
0.84	4.3430	419 (0.93)	12.0	97.7 (0.77)	5.3
0.86	4.5170	382 (0.94)	7.8	39.0 (0.84)	3.9

Metal oxide film becomes more conducting with increasing potential.

EIS Tafel Analysis

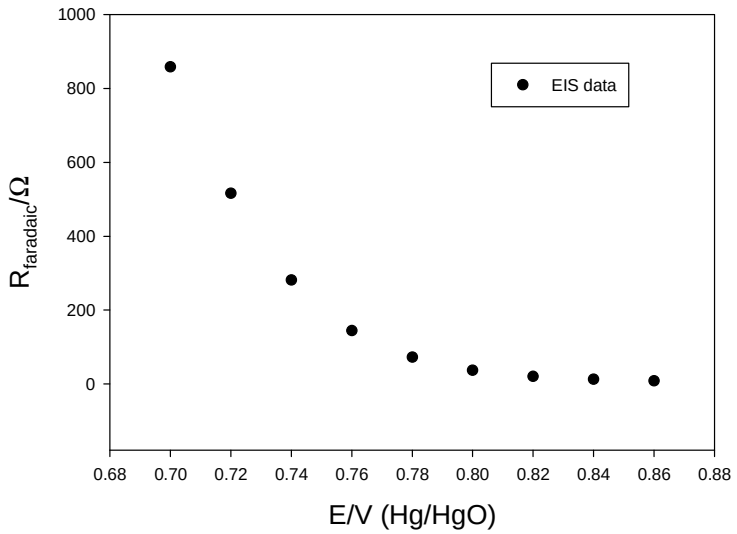

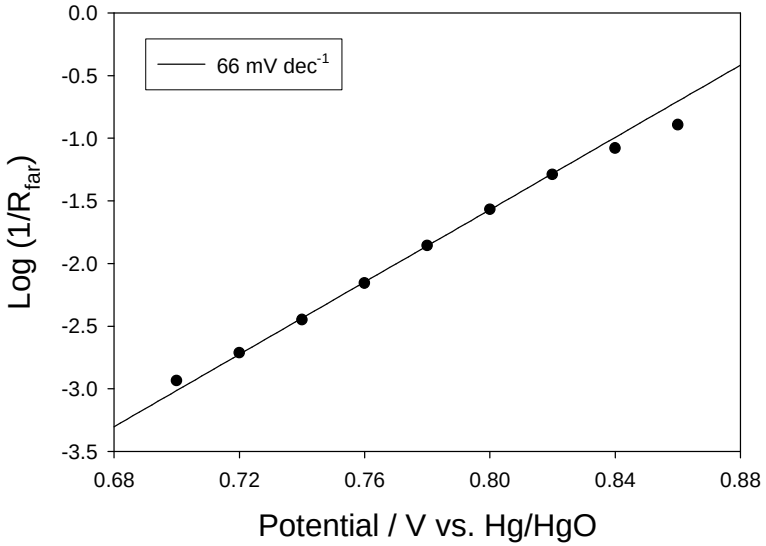

•At OER overpotentials where simple Tafel behaviour prevails:

$$i = i_0 \exp\left(\frac{2.303\eta}{b}\right)$$

Differentiating gives:

$$\frac{di}{d\eta} = \frac{2.303 i_0}{b} \exp\left(\frac{2.303\eta}{b}\right)$$

Noting that $di/d\eta = di/dE = 1/R_{far}$:

$$\log\left(\frac{1}{R_{far}}\right) = \frac{E}{b} + \log\left(\frac{2.303 i_0}{b}\right)$$

•EIS Tafel slope 66 mV dec^{-1}

•Good agreement with steady-state polarisation Tafel slope of 60 mV dec^{-1}.

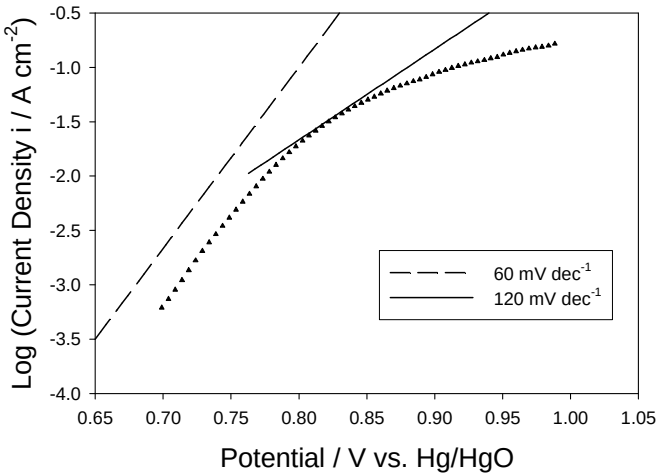

Tafel Plots OER, alkaline solutions. Electro-precipitated Nickel oxy-hydroxide thin films deposited via CPM on Au supports.

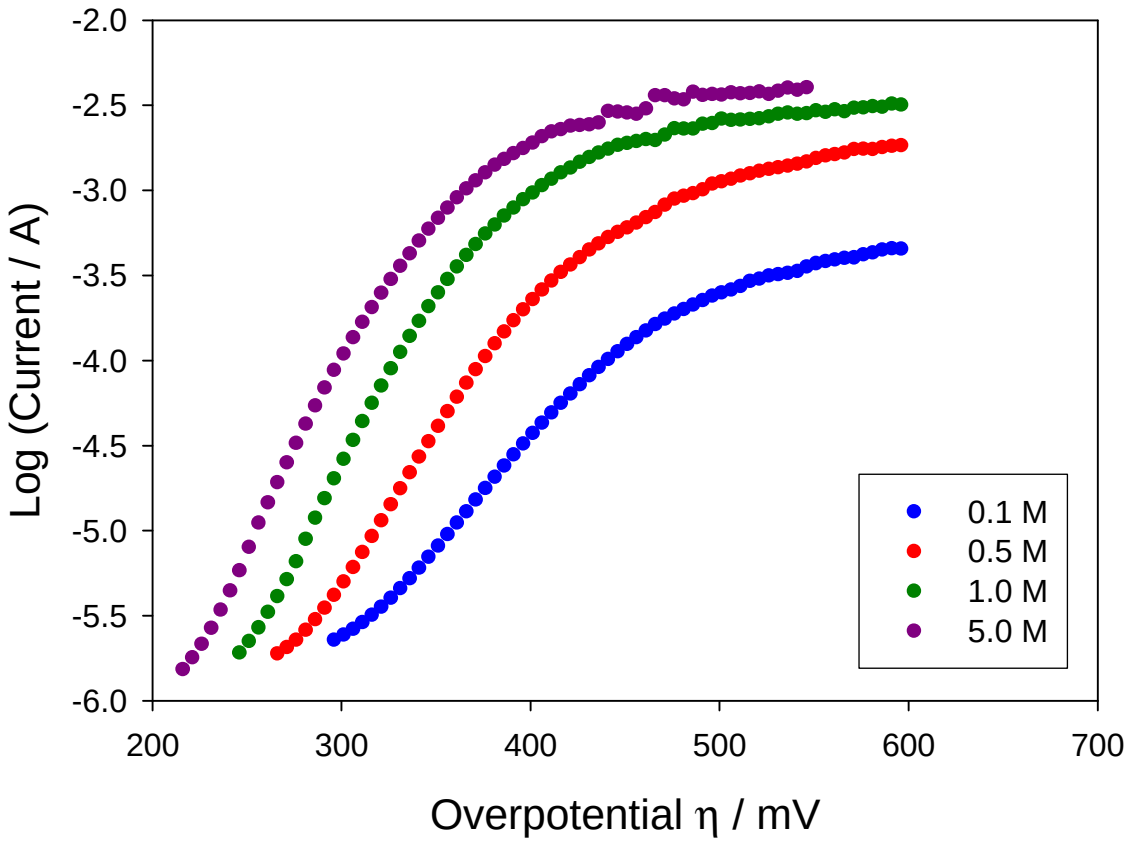

OER onset overpotential decreases with increasing base concentration.

Low potential Tafel slope for OER at electro-precipitated nickel oxyhydroxide film grown on Au support via CPM, as function of OH^- concentration.

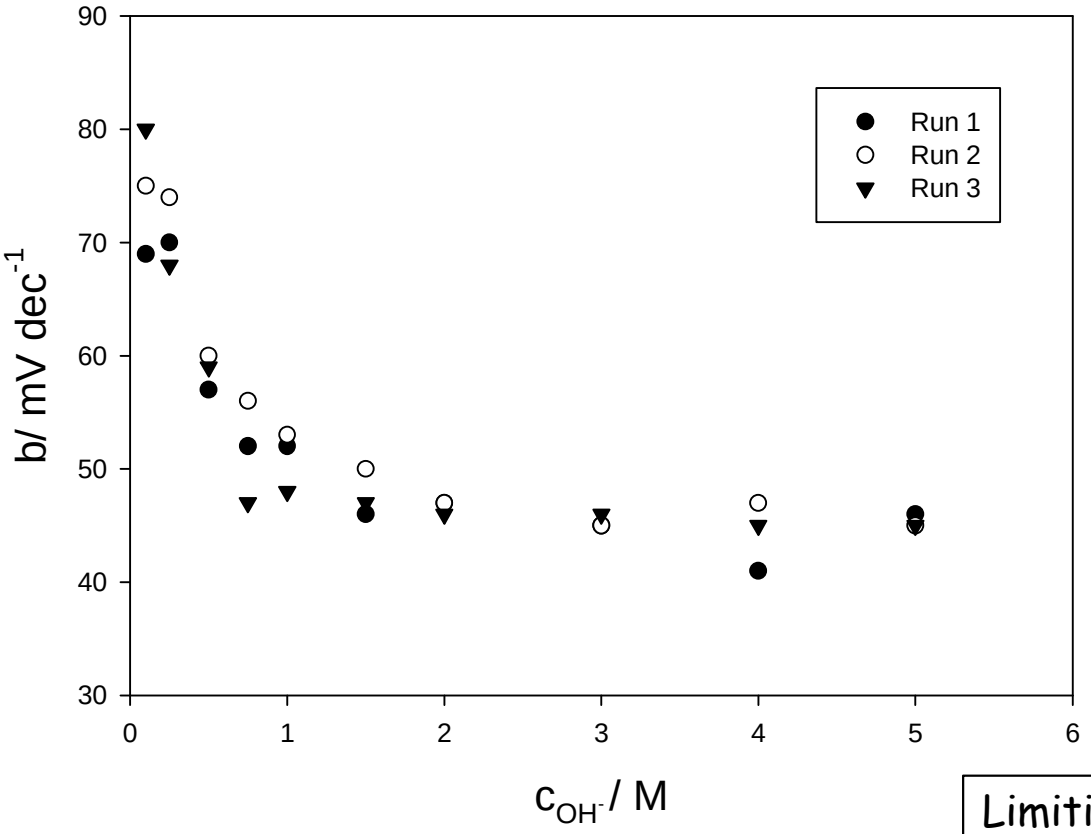

Limiting low potential
TS = 47 mV/ dec

N = 30 cycles SR = 50 mV s^{-1} Plating medium: 0.1 M $NiSO_4$, 0.1 M $NaAc.3H_2O$, 0.001 M KOH
CPM : - 900, + 1200 mV (vs SCE), 50 mVs^{-1}.

High potential Tafel slope for OER at electro-precipitated nickel oxyhydroxide film grown on Au support via CPM, as function of OH^- concentration.

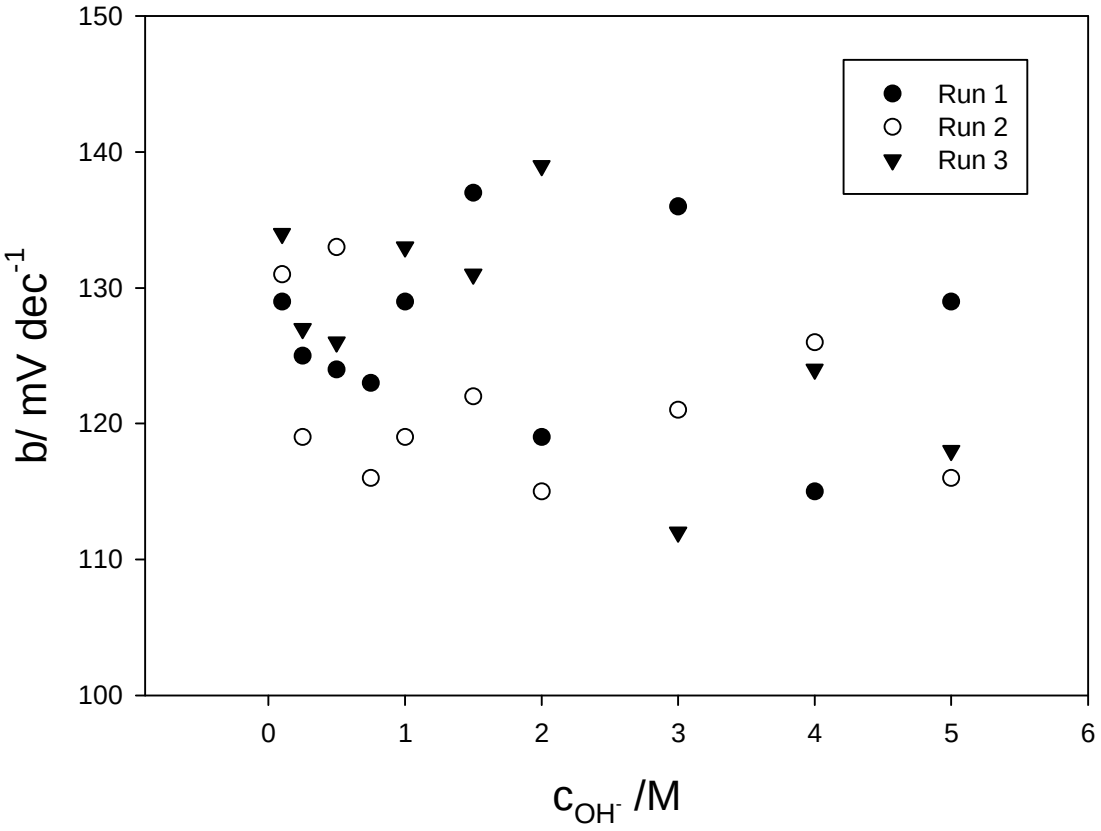

Reaction order plot. Electroprecipitated Nickel oxy-hydroxide thin films.

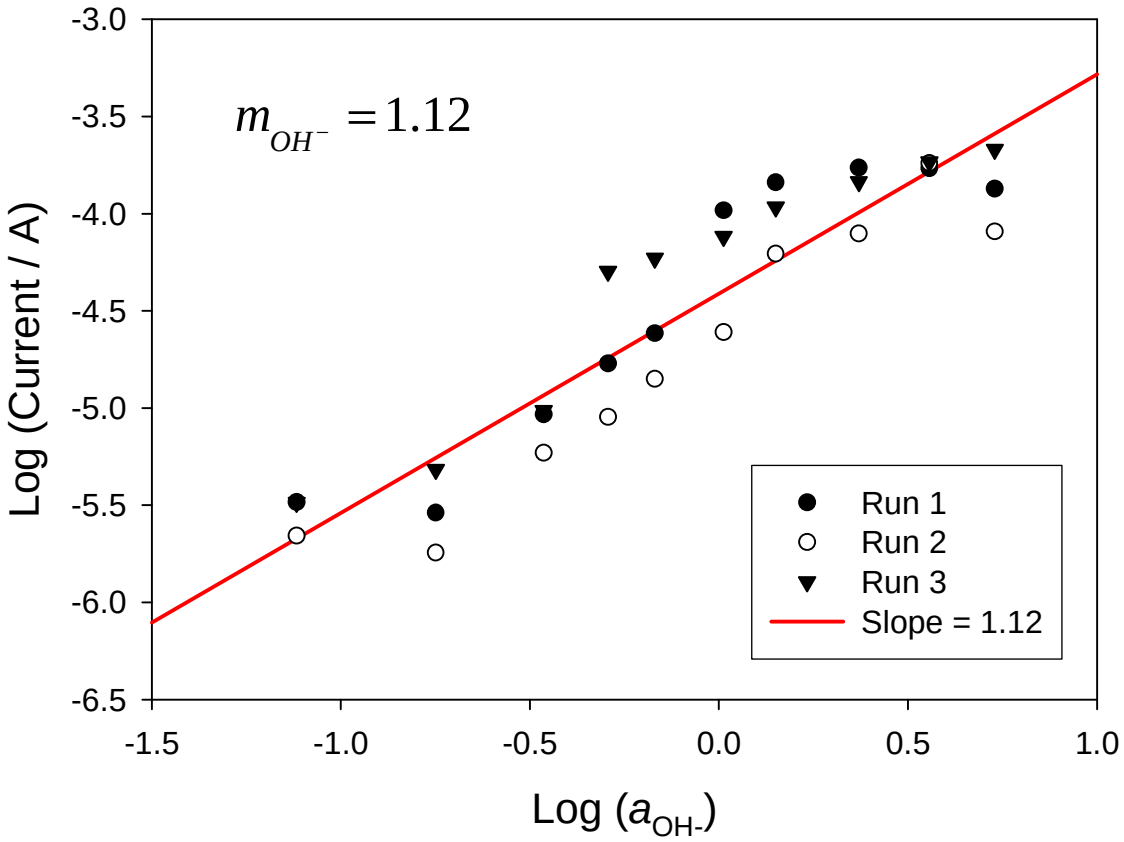

OER Mechanism at Fe & Ni oxyhydroxide modified electrodes

S = surfaquo group attached to oxide lattice via bridging oxygen ligands.

$$SOH_2 + OH^- \rightleftharpoons SOH^- + H_2O$$

$$SOH^- \rightarrow SOH + e^-$$

$$SOH + OH^- \rightarrow SO^- + H_2O$$

$$SO^- \rightarrow SO + e^-$$

$$SO + OH^- \rightarrow SOOH + e^-$$

$$SOOH + OH^- \rightarrow SO_2 + H_2O + e^-$$

$$SO_2 + OH^- \rightarrow O_2 + SOH^-$$

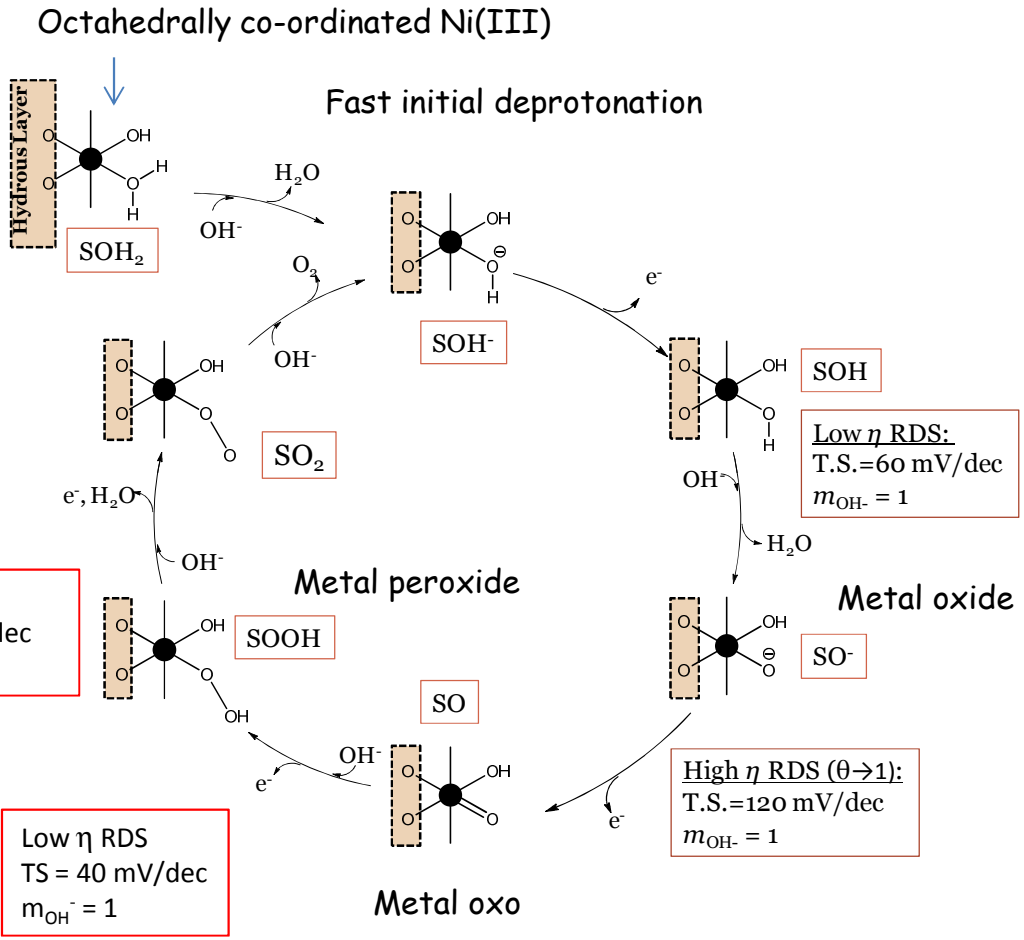

DFT calculations being initiated to generate quantitative Energy Landscape for OER Mechanism.

Mechanism valid for multicycled & electroprecipitated M = Fe & Ni.
Explains Tafel Slope & reaction order data.

Similar mechanism applicable for DSA films

OER mechanism involving surfaquo groups in the hydrous oxy-metal hydroxide layer.

An atlas of electrochemical reactivity for anodic OER

Electro-precipitated β-$Ni(OH)_2$: The 'right' type of oxide for OER

Tafel Plots IR Corrected.

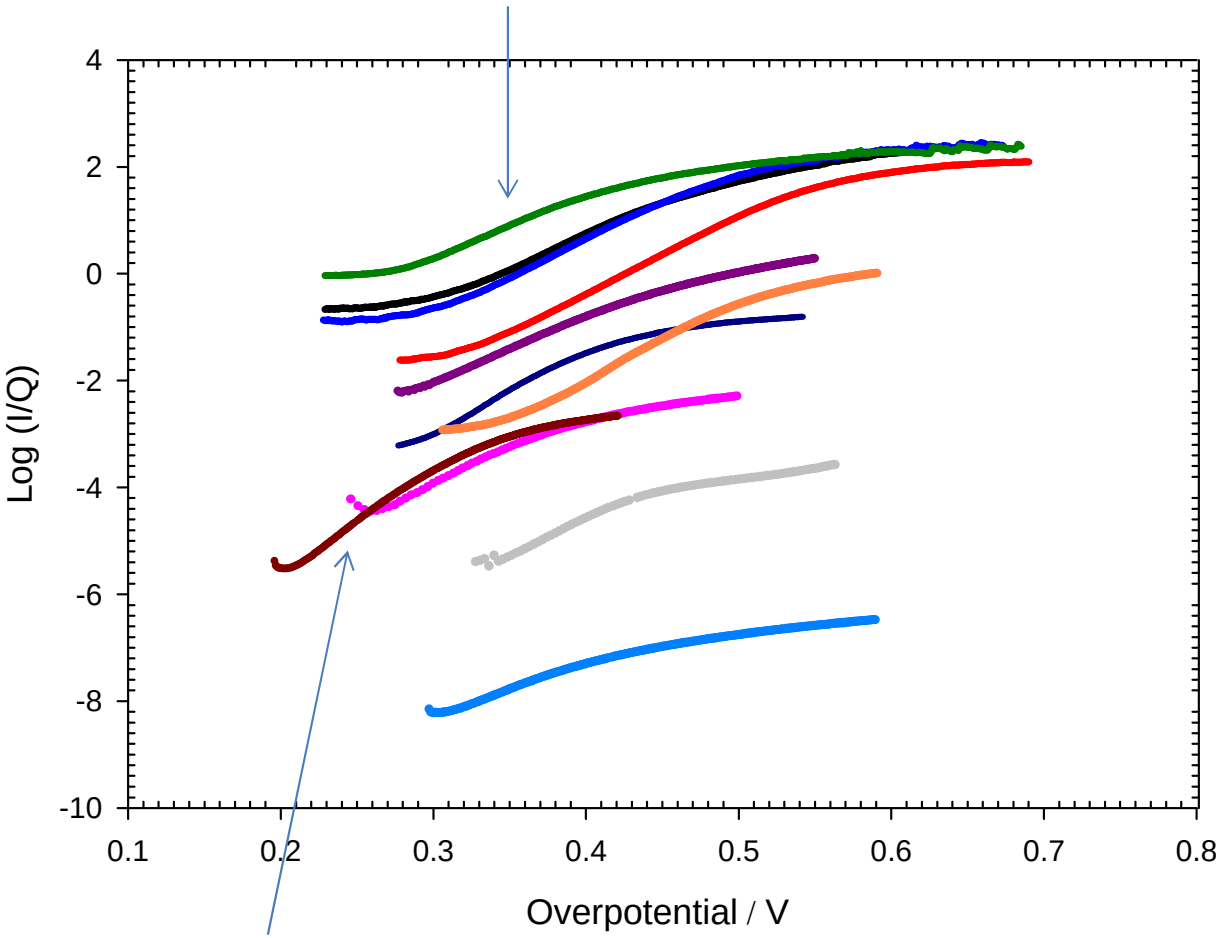

We have succeeded in preparing very effective catalytic electrodes for anodic OER using very cheap Materials (nickel oxide).

Current DSA 'state of art'

All currents (OER rate) scaled to voltammetric charge which is proportional to real surface area.

- Electrodep $Ni(OH)_2$ on Pt
- Electrodep $Ni(OH)_2$ on GC
- Electrodep $Ni(OH)_2$ on Au
- Electrodep aged Ni(OH) on Au
- Hydrous Nickel Oxide 120 cycles
- Hydrous Iron Oxide 120 cycles
- Thermally prepared NiO on Ni Substrate
- Thermally prepared RuO2 Ni substrate
- Thermally prepared RuO2 on Ti substrate
- Thermally prepared Rh2O3 on Ni substrate
- Thermally prepared Rh2O3 on Ti substrate

An atlas of electrochemical reactivity for anodic OER

Tafel Plots IR corrected and normalised wrt real surface area S measured via electrochemical capacitance measurement.

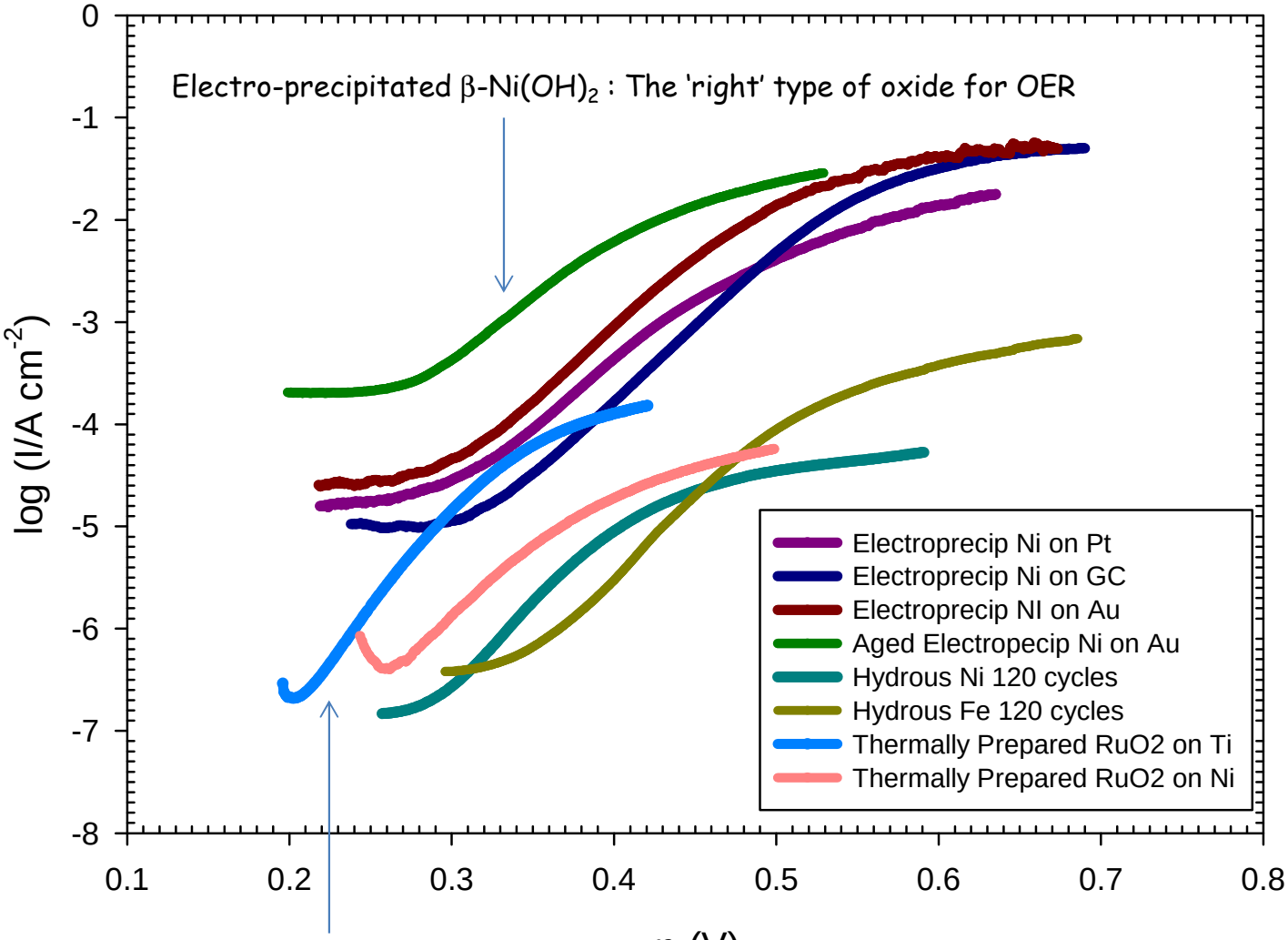

Concluding Comments

- Reproducible and scalable methodology developed for generation of hydrated Fe & Ni metal oxide thin films and electroprecipitated nickel oxyhydroxide films on Au, GC and Pt supports in aqueous base.
- Duplex layer model proposed for structure of oxide/solution interface region.
- Hydrous oxide thin films exhibit super-Nernstian shifts in redox potential with respect to changes in solution pH value. Implying commercial spinoff potential for new generation metal wire pH sensors for use in biomedical applications.
- Dynamics of redox switching in hydrous oxide layer quantified via Aoki Model.
- Electro-catalytic kinetics and mechanism with respect to anodic OER at Ni and Fe electrodes in aqueous base evaluated and quantified.
- Novel anodic water splitting OER mechanism proposed involving surfaquo groups in hydrous oxide layer. OER onset potential depends on acid/base properties of hydrous oxide layer.
- Currently developing molecular scale model for detailed OER pathway in terms of interlinked surfaquo group model.
- Fe and Ni oxide materials are cheap and effective electrode materials for anodic water splitting.
- Next stage is to examine application of these oxide materials to Cathodic Oxygen Reduction Reaction (ORR) and hydrogen evolution reaction (HER). The latter topics are currently unexplored at hydrous oxide materials.
- Extending analysis to metal oxide films prepared via thermal decomposition of precursor & via sol/gel routes.